The Science and Technology of Rubber

Fourth Edition

Edited by

Burak Erman
Department of Chemical and Biological Engineering
Koc University
Rumeli Feneri Yolu 34450 Istanbul, Turkey

James E. Mark
Department of Chemistry
University of Cincinnati
Cincinnati, OH 45221-0172, USA

C. Michael Roland
Naval Research Laboratory
Chemistry Division, Code 6120
Washington, DC, USA

Notices
Knowledge and best practice in this field are constantly changing. As new research and experience broaden our understanding, changes in research methods, professional practices, or medical treatment may become necessary.

Practitioners and researchers must always rely on their own experience and knowledge in evaluating and using any information, methods, compounds, or experiments described herein. In using such information or methods they should be mindful of their own safety and the safety of others, including parties for whom they have a professional responsibility.

To the fullest extent of the law, neither the Publisher nor the authors, contributors, or editors, assume any liability for any injury and/or damage to persons or property as a matter of products liability, negligence or otherwise, or from any use or operation of any methods, products, instructions, or ideas contained in the material herein.

For information on all Academic Press publications
visit our website at http://store.elsevier.com

Working together
to grow libraries in
developing countries

www.elsevier.com • www.bookaid.org

Structure Characterization in the Science and Technology of Elastomers

C.M. Roland

Naval Research Laboratory, Chemistry Division, Code 6120, Washington, DC, USA

3.1 INTRODUCTION

Early structural characterization of polymers focused on solution properties and their relationship to molecular weight (Dawkins, 1986; Booth and Price, 1989; Yamakawa, 1971; Flory, 1969). Subsequently spectroscopic and chromatographic techniques were developed, and reviews are widely available (Tanaka, 1991; Campbell and White, 1989; Baldwin and Ver Strate, 1972; Hsu, 2004; Stuart, 2002; Koenig, 1999). This chapter describes various characterization techniques, including discussion of the classical methods of analysis, as well as NMR, SANS, and so on. The main modifications for the fourth edition include the addition of newer methods and results and an update of the references.

Knowledge of chemical structure (backbone composition, compositional and sequence distribution) and the macrostructure of a rubber (molecular weight and its distribution, the degree and type of branching) allows inferences to be drawn concerning the mechanical properties (Chapters 4, 5, and 10), the rheology (Chapters 6 and 14), curing behavior (Chapter 7), filler reinforcement (Chapter 8), and chemical reactivity (Chapter 11). However, relationships between fundamental molecular variables and the properties of condensed matter are semiquantitative at best, and correlation never guarantees causation. Following the earlier editions, methods for molecular weight determination are discussed at greater length than spectroscopic methods. This bias is based on the idea that areas in which common problems might arise, with individuals making their own data interpretation, should receive greater attention.

3.2 CHEMICAL COMPOSITION

Elemental analysis of polymers, which refers to determination of the elements and their respective quantities comprising the material, can often be carried out by the methods used for low molecular weight organic compounds (Dawkins, 1986; Booth and Price, 1989; Stuart, 2002; Braun, 1996; Mitchell, 1992; Collins et al., 1973; Tyler, 1967). This is particularly true for methods involving combustion of the sample. Thus, C, H, and N can be determined on milligram samples by complete combustion followed by gas chromatographic analysis of the evolved gases. Sulfur and halogens are also easily determined after combustion, by titration of sulfate or SO_2 for S, and by potentiometric titration with $AgNO_3$ for halogens after treatment of the gases with NaOH and hydrazine sulfate, for example. Interference by nitrogen on sulfur tests can be a problem. Quantities as low as ppm metals can be determined quickly by X-ray techniques.

Elemental analysis reveals only which atoms are present. Determination of the chemical structure usually requires spectroscopic methods. The moieties in the polymer absorb and emit radiation at characteristic frequencies. Skeletal bond transitions can be detected in the infrared and Raman spectra, electronic transitions typical of unsaturated bonds correspond to ultraviolet and visible wavelengths, atomic nuclei with magnetic moments are probed using magnetic resonance experiments.

For basic information, infrared spectroscopy (Hsu, 2004; Stuart, 2002; Koenig, 1999; Ishida, 1987; Messerschmidt and Harthcock, 1988) (invariably Fourier transform infrared, FTIR) is a straightforward technique. Thin films of elastomers, obtained by casting or molding 20–30 mg of sample, can be measured directly. Most analyses make use of the mid-infrared region (4000–400 cm^{-1}), with sample identified by comparisons using widely available spectral libraries (Hsu, 2004; http://www.spectroscopynow.com). If the polymer is crosslinked, it must be microtomed, or spectra obtained in reflection, most commonly using attenuated total reflection (ATR) (Fuhrmann and Karger-Kocsis, 2003; Shield and Ghebremeskel, 2003; McCarley and Bunge, 2003; Rodrigues et al., 2001; Sen et al., 2001) or photoacoustic FTIR (Peckj et al., 1991; Waddell and Parker, 1992). The latter refers to the measurement of sound arising from the selective absorption of modulated light. The sample surface is heated by the absorption, which in turns heats the adjacent air, producing an alternating pressure wave. Sub-milligram-sized samples can be analyzed using infrared microscopy (Messerschmidt and Harthcock, 1988; Stebounova et al., 2003; Keilmann, 2003, 2002; Dumas, 2003; Wetzel and LeVine, 1999; Palanker et al., 2000; Kempfert et al., 2001; Froud et al., 2003; Szep et al., 2003; Maeda et al., 2003; Berger et al., 2003).

Raman spectroscopy yields analogous information and is complementary to infrared spectroscopy. At least for molecules with a center of symmetry, vibrations that are infrared inactive are generally Raman active, and vice

versa. Since the detected light is scattered rather than transmitted by the sample, Raman spectra are readily obtained on crosslinked specimens, and the method has been applied to the study of rubber vulcanization (Tanaka, 1991; Koenig, 1999; Zhao et al., 2006). Interferences due to fluorescence can be avoided by using a longer wavelength source (Rabolt and Chase, 2000). Spatial resolutions of a few hundred nanometers can be achieved using Raman microscopy (Ghanbari-Siahkali et al., 2003; Zerda et al., 2003; Dieing et al., 2011; Smitthipong et al., 2008; Wang et al., 2011).

Whereas Raman and infrared are useful for "fingerprinting" (i.e., identifying chemical structure), extension of the spectroscopic measurements into the visible and ultraviolet (UV) regions is done primarily for quantitative analyses (Grum, 1972; Raubner et al., 2002; Braun et al., 1993). Extinction coefficients for conjugated unsaturated structures are very large.

The foregoing spectral absorption methods can yield quantitative results, although calibration is required. With nuclear magnetic resonance spectroscopy (NMR) (Koenig, 1999; Stuart, 2002; Cheng, 1991; Kinsey, 1990; Wang et al., 1993), the absorption intensity is directly proportional to the amount of the particular isotope present; consequently, ratios of absorption intensities in proton NMR, for example, can be used to determine the number of chemically distinct protons in a sample. The characteristic NMR resonance frequency (e.g., "chemical shift") depends on chemical environment, and therefore the specific chemical nature of the material can be identified.

Chemical information obtained using ^{1}H and ^{13}C NMR is usually obtained on samples in solution (liquid-state NMR) in order to improve resolution. However, ^{13}C spectra can also be obtained on neat specimens, such as rubber. This is possible as long as there is sufficient molecular motion to average the orientation-dependent variation in chemical shift of chemically identical atoms (chemical shift anisotropy, CSA). Chemical shifts in ^{13}C NMR spectra span a much wider range than in proton NMR, and therefore the former provides better spectral resolution. However, the Nuclear Overhauser effect (NOE) and other nuclear relaxation processes cause the ^{13}C absorption intensities to deviate from direct proportionality to the number of carbon atoms. Thus, unless specific techniques are utilized, ^{13}C NMR spectral intensities using standard liquid-state NMR acquisition methods are not quantitative.

This is also true when applying solid-state NMR techniques (Kinsey, 1990) to obtain high-resolution ^{13}C spectra of more rigid samples. Using a combination of magic angle spinning (MAS) and proton decoupling (via high power radiofrequency irradiation of proton resonances), the line-broadening effects of CSA and ^{13}C-proton dipole-dipole interactions can be removed. Relatively high-resolution ^{13}C NMR spectra can be obtained, and these methods can be used for various investigations of cured elastomers (Madan et al., 2012; Litvinov et al., 2011; Wu et al., 2011; Goga et al., 2008; Kotani et al., 2007).

NMR not only yields chemical information, but can also be used to analyze polymer tacticity, sequence lengths, short-chain branching, and crystallinity.

From elemental analyses, infrared, and NMR methods, the chemical repeat units, including blockiness, can be determined, although quantification is more difficult for low concentrations of a monomer unit or functional group, or for atoms other than C and H. An alternative approach is based on the chemical reactivity of the particular group (Smith and Patterson, 1986), although the reaction may be slow due to the low concentration of the group. Examples include acid groups titrated with base; quantitative addition reactions of many olefins with ozone or halogens; esterification of hydroxyl groups with anhydrides, with subsequent titration to evaluate hydroxyl content. In many cases, the procedure has been established for small molecule materials.

Pyrolysis (Hammond and Lehrie, 1989; Vitalini and Scamporrino, 1992; Ghebremeskel et al., 1996; Yamada et al., 1991; Schulten et al., 1989) of samples can produce characteristic fragments, which may be analyzed by gas chromatography (GC) (Stuart, 2002) or mass spectrometry (MS) (Lattimer, 1990). Since the relationship between fragments and the original polymer is often complex, this technique is a last recourse, applied, for example, to insoluble polymers. Combined GC/MS has been used to analyze the volatile components in natural rubber (Hoven et al., 2003). In ozonolysis (Stuart, 2002), an unsaturated sample is reacted to form an unstable intermediate, ozonide, which is then further reacted for chemical identification. Ozonolysis of rubber is usually combined with GC analysis (Kawahara et al., 1998; Tanaka et al., 1987; Tanaka and Sato, 1986; Miller and Tobias, 1978). In secondary ion mass spectrometry (SIMS), the sample surface is irradiated with an ion beam, followed by mass spectrometry of the emitted secondary ions (Leeson et al., 1997; Ruch et al., 2003; van Gennip et al., 2004). SIMS has found various applications in rubber (Ruch et al., 2003; Winesett and Tsou, 2008) including surface analysis (Fulton, 2006; Van Ooij and Rangarajan, 1988; Briggs, 1989) and studies of carbon black interaction (Mathew et al., 2008; Betrand et al., 2002; Betrand and Weng, 1999). Pyrolysis can also serve as a fingerprinting technique for routine analyses. In thermogravimetric analysis (TGA) (Sircar, 1992, 1997), the polymer degradation by-products volatize, whereby the residue provides a measure of the carbon black or other filler content.

Electron paramagnetic resonance (EPR), or electron spin resonance (ESR), can be used to detect types and quantities of free radicals. Such information is of value in studying the chemistry occurring during degradation and fracture of polymeric materials (Capancioni et al., 2003; Hauck et al., 1997; Hinojosa et al., 1972; Devries, 1971; Partridge et al., 1993; Pace and Roland, 1991). EPR can also be applied to study carbon black and other fillers in polymers (Brosseau et al., 2001; Tang et al., 1994; Hommel et al., 1993).

3.3 SEQUENCE DISTRIBUTION OF REPEAT UNITS

Elastomers are usually comprised of various additives (a typical formulation includes more than a dozen ingredients), as well as possible impurities. Additionally, the polymer itself may be a copolymer of different monomer units, or the rubber may be a blend of two or more polymers. In order to determine whether the elastomer contains additives or impurities, or is itself heterogeneous, the components of the mixture must be separated (i.e., fractionated). Many methods are available to separate components, with the latter then identified by techniques such as those shown in Table 3.1. Precipitation and/or dissolution methods simply rely on differences in solubility of the components (Ver Strate et al., 1988). If the molecular weight distribution is broad, a fractionation scheme is combined with one of the more sophisticated analyses described later. If there is intramolecular heterogeneity, "cross" or "orthogonal" fractionation, which requires at least two fractionation mechanisms, may be needed.

The technique of temperature rising elution fractionation (TREF) (Garcia et al., 2011; Feng and Hay, 1998; Mirabella, 1993; Wild, 1991) has been

TABLE 3.1 Characterization of Chemical Composition

Technique	Principle of Operation
Elemental analysis	Analysis of products of decomposition
Infrared absorption $1 < \lambda(\mu m) < 16$	Characteristic vibrational frequencies
Raman scattering	Characteristic vibrational frequencies
Nuclear magnetic resonance (NMR)	Characteristic transition energies of any nucleus with a magnetic moment (^{1}H, ^{2}H, ^{13}C, ^{129}Xe, etc.)
Ultraviolet (UV) and visible light absorption $0.2 < \lambda(\mu m) < 0.8$	Characteristic energies of electronic transitions
Functional group analysis	Analyze for known reactions of chemical moiety
Pyrolysis/ozonolysis	Pyrolysis with chromatographic or mass spectrographic identification of fragments
Electron paramagnetic resonance (EPR)	Energy of unpaired electron spin transitions, which depends on chemical environment
Thermogravimetric analysis (TGA)	Weight loss due to temperature-dependent decomposition and evaporation
Mass spectrometry (MS)	Mass of fragments reflects chemical composition
Secondary ion mass spec (SIMS)	Characteristic ions emitted from surface

developed to measure the compositional distribution of semicrystalline polymers. Polymer is dissolved off a substrate as temperature is raised through the melting region, so that discrimination is based on differences in crystallizability of the fractions. A similar method uses supercritical fluids (Dekmezian et al., 1990). TREF can provide information about the sequence distribution, since longer sequences of a stereoregular repeat unit are more crystallizable.

Size exclusion chromatography (SEC) (Stuart, 2002; Ruckebusch et al., 2008; Zimina et al., 1992; Dekmezian et al., 1990; Grubsic-Gallot et al., 1990), also referred to as gel permeation chromatography, utilizes differences in hydrodynamic volume. It is discussed in more detail later. A very basic technique is adsorption chromatography (Glockner, 1989; Xu et al., 2000), in which separation arises from variation in the retention of the chain units or functional groups in a mobile phase, due to their interaction with a stationary surface. Other techniques rely on rates of sedimentation (Yamada et al., 1997; Stanley and Strey, 2003) and diffusion-adsorption phenomena (thin layer chromatography, TLC) (Tacx et al., 1988; Mori and Mouri, 1989).

Different arrangements of the monomer units give rise to different chemical shifts and scalar couplings (splittings) in the NMR spectra. Using selection rules and empirical knowledge of chemical shifts, chemical structures can be assigned. Since chemical shifts in ^{13}C NMR spectra are larger than in proton spectra, subtle structural differences can be seen for carbon atoms separated by up to five bonds from the point of difference. Thus, ^{13}C NMR can be very useful for determining the distribution of chain units in the polymerz backbone. An example of this is seen in Figure 3.1, which shows ^{13}C NMR
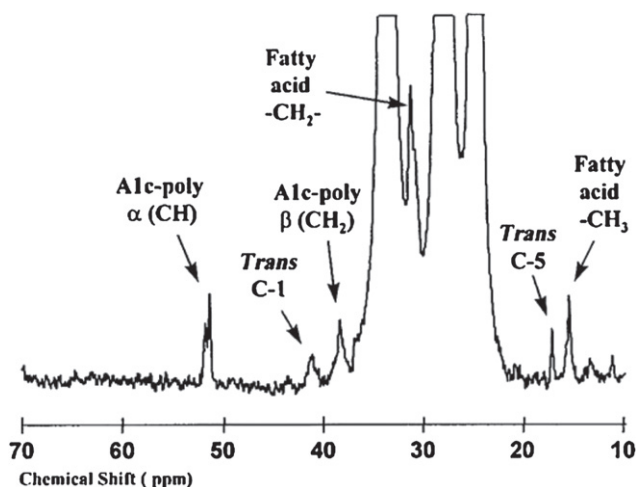

FIGURE 3.1 Magnified portion of ^{13}C NMR spectrum of natural rubber vulcanized to half its maximum torque. The peak at 16 ppm arises due to cis-to-trans isomerization (Mori and Koenig, 1998).
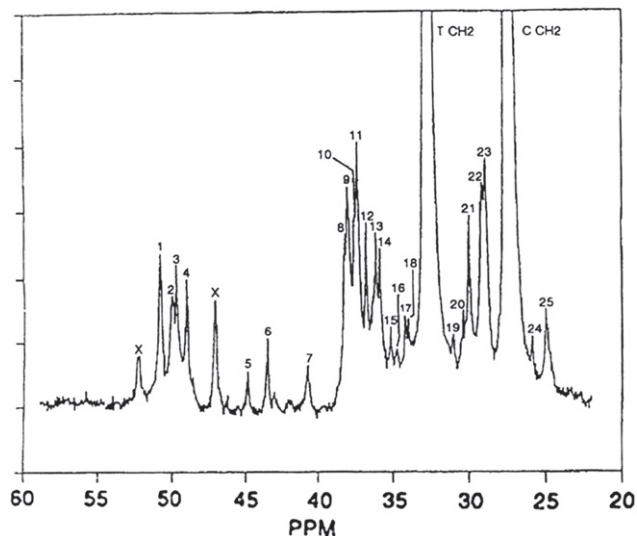
FIGURE 3.2 Magnified ^{13}C NMR spectrum of *cis*-1,4-polybutadiene after curing. The arrows designate new peaks appearing due to the vulcanization. The first seven represent methine carbons and the other 18 are due to methylene carbons (Clough and Koenig, 1989).

spectra of sulfur-cured natural rubber (NR) reinforced with carbon black (Mori and Koenig, 1998). There is a small peak reflecting the *trans* isomer content, which grows in intensity as the vulcanization proceeds. Thus, the NMR measurements yield quantitative information about the extent of *cis-trans* isomerization accompanying the curing of NR. Similar results are found for *cis*-1,4-polybutadiene rubber (Zaper and Koenig, 1988; Clough and Koenig, 1989; Koenig, 2000). Figure 3.2 illustrates the plethora of changes in the NMR spectrum accompanying curing.

Differences in the arrangement of monomer units along the chain backbone are another form of heterogeneity. Chemically different monomer units may occur in sequences of varying length, while identical monomer units can have different geometrical arrangement (stereoisomers), yielding different properties. The stereo-regularity of the polymer can often be determined using the same techniques employed for chemically distinct units, with NMR and infrared the most useful.

When the sequences in the copolymer are longer than 6–8 carbons, techniques other than NMR are needed to directly determine their length. The use of pyrolysis followed by GC-MS analysis has been proposed to find the long sequences as fragments in the pyrolyzate, but the data produced are complicated and difficult to interpret (Tosi, 1968; Yamada et al., 1990; Tulisalo et al., 1985; Hu, 1981).

3.4 CHAIN ARCHITECTURE

The viscoelastic response of amorphous polymers at elevated temperatures is governed to a significant extent by the weight average molecular weight, M_w, the presence of any long chain branching, and the MWD (Tuminello et al., 1993; Graessley and Ver Strate, 1980; Doi, 1993; Ngai and Plazek, 1995; Wasserman, 1995; Majeste et al., 2003). Even the properties of cured elastomers may reflect the length of the original chains, since chain ends, whose concentration is inversely proportional to the number-average molecular weight M_n, represent defects.

3.4.1 Molecular Weight and Its Distribution

The chain length distribution is usually presented as a plot of the mole fraction or weight average of molecules versus molecular weight. The various average molecular weights represent the moments of the chain length distribution

$$\overline{M}_j = \sum_{i=1}^{\infty} N_i M_i^{j} \left/ \sum_{i=1}^{\infty} N_i M_i^{j-1} \right., \tag{3.1}$$

where $i = 1, 2,$ and 3 yield the number average M_n, weight average M_w, and z average M_z, respectively. For a uniform distribution of chain lengths, $M_n = M_w = M_z$. The common random MWD gives $M_w/M_n = 2$ and $M_z/M_w = 1.5$, while for the Schulz-Zimm distribution, $M_n + M_z = 2M_w$ and $1 < M_z/M_w < 2$. Figure 3.3 shows a typical molecular weight distribution.
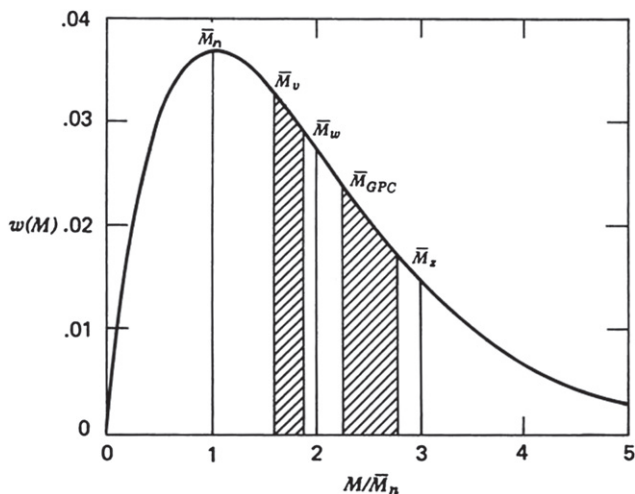

FIGURE 3.3   Representative molecular weight distribution. $M_{GPC} = \sum w_i M_i^{1+a} / \sum w_i M_i$, where a is the Mark-Houwink exponent (Collins et al., 1973).

The number-average molecular weight determines the colligative properties (i.e., those that depend only on the number of dissolved molecules) of polymer solutions (Table 3.2). Measurements of freezing point depression (cryoscopy) or boiling point elevation (ebulliometry), in principle, will yield the same information for macromolecules as for small molecules (Bonnar et al., 1958; Barth and Mays, 1991; Cooper, 1989). These are absolute techniques, which do not require calibration. The change in (melting or boiling) temperature, ΔT, follows a relationship of the form

$$\Delta T/kc = M_n^{-1} + A_1 c + A_2 c^2 + \cdots, \tag{3.2}$$

where c is the concentration, A_i are the virial coefficients, and k is a constant that depends on the solvent, temperature, and the instrument. The number of moles of macromolecules present at mass concentrations sufficiently low to obtain ideal solutions is very small. Therefore, the anticipated change, ΔT, in boiling or freezing points is correspondingly small; for $M_n = 10^5$ g/mol, $\Delta T \sim 10^{-5}$–10^{-4} °C. Thus, these classic techniques are not used above $M_n \sim 10^4$ g/mol. Moreover, cryoscopy and ebulliometry are time consuming and have poor accuracy.

For low molecular weight samples, the preferred method is by vapor pressure osmometry (VPO) (Barth and Mays, 1991; Cooper, 1989). This technique is based on the decrease of vapor pressure of a solvent due to the presence of dissolved polymer. The different equilibrium vapor pressures cause a difference in condensation rate on two matched thermistors, contained in a chamber saturated with solvent vapor. One thermistor is coated with solvent and the other with a solution of the polymer. More solvent condenses on the solution, raising its temperature. The consequent temperature difference is measured, and by calibration, M_n can be determined. VPO is fast and can yield M_n as high as about 5×10^4 g/mol. Commercial vapor pressure osmometers are available.

Membrane osmometry (Barth and Mays, 1991; Cooper, 1989; Brown and Verdier, 1972) relies on the lowering of the activity (free energy) of the solvent by dissolution of a solute, to yield a direct determination of M_n. When a polymer solution is brought in contact with pure solvent, the concentration gradient induces mixing by diffusion. If a semipermeable membrane is placed between the pure solvent and solution, the polymer is trapped but solvent can pass. Equilibrium cannot be attained, but if the polymer solution is in a closed cavity, a pressure develops on the solution side, which eventually stops the solvent flow. The magnitude of this "osmotic" pressure, Π, will depend only on the number of polymer molecules present, at least in the absence of polymer-polymer interactions (i.e., at low concentrations). The equation relating these quantities is analogous to the relation above for the change in melting and boiling points. Measurements at several concentrations with extrapolation of Π/c to $c = 0$ yields M_n. Even for high molecular weight materials, the osmotic pressure is significant. For a 1% solution of a material of $M_n = 10^5$ g/mol,

TABLE 3.2 Characterization of Molecular Weight and Its Distribution

Technique	Variables Measured	Principle of Operation	Range (g/mol)
Membrane osmometry (MO)	Number average molecular weight; virial coefficient	Osmotic pressure due to diffusion of solvent through membrane impermeable to polymer	
Vapor pressure osmometry	Number average molecular weight	Vapor pressure lowering	$<5 \times 10^4$
Cryoscopy	Number average molecular weight	Freezing point depression	$<10^4$
Ebulliometry	Number average molecular weight	Boiling point elevation	$<10^4$
Light scattering (LS)	Weight average molecular weight	Light scattering intensity from solution is proportional to the molecular weight of the solute	$>10^3$
	Virial coefficient		
	Radius of gyration	Angular dependence related to particle size	
Neutron scattering	Weight average molecular weight	Scattering intensity is proportional to nuclear cross section	
	Virial coefficient		
	Radius of gyration		
Intrinsic viscosity	Intrinsic viscosity	Solution viscosity depends on polymer molecular weight	$>10^3$
	Viscosity average molecular weight		
Size exclusion (SEC) or gel permeation (GPC) chromatography	Molecular weights and distribution	Permeation of polymer from a flowing solution into a porous stationary phase	$<10^7$
Field flow fractionation (FFF)	Molecular weights and distribution	External field effects separation of flowing solute	$<10^7$
Ultracentrifugation	Molecular weight averages	Concentration gradient in a large gravitational field is related to molecular weights	$>5 \times 10^2$
Sedimentation	Molecular weights	Rates of diffusion in a gravitational field related to molecular weights	$>5 \times 10^2$
	Sedimentation coefficient		
Melt viscosity	Dynamic or steady-state viscosity	Empirical correlation of viscosity and M_w	–

the pressure is about 250 Pa at 25 °C. Generally, the technique is useful for molecular weights in the range from 10^4 to almost 10^6 g/mol.

A frequent difficulty with the method is that Π/c may become nonlinear in c for higher concentrations. If this is due to agglomeration, solvent or temperature changes can sometimes eliminate the problem. To get measurable osmotic pressures for larger M_n, the range of c must be increased. A_2 decreases with M_n in good solvents ($A_2 \sim M^{-0.2}$), but not as fast as c is increased. Therefore, nonlinear plots are often encountered when studying high M_n samples. In order to linearize the data, $(\Pi/c)^{1/2}$ can be plotted versus c. The greatest difficulties with this method relate to imperfections in the membrane. Sometimes the polymer can diffuse through the membrane, with steady-state values indicating permeation of molecules having $M < 5 \times 10^3$ g/mol. This can lead to significant errors, ca. 10%, and even larger for distributions skewed to low molecular weights.

Light scattering is another absolute technique for the determination of molecular weights ($>10^3$ g/mol) (Stuart, 2002; Barth and Mays, 1991; Cooper, 1989; Tanaka, 1999; Berne and Pecora, 1976; Boothroyd and Fetters, 1991; Schulz et al., 1957; Casassa, 1972; Shultz and Stockmayer, 1969; Suzuki et al., 1973). (We are only concerned with static light scattering for structural information; however, inelastic light scattering is a powerful technique for studying polymer dynamics. From calibration, it can also yield molecular weight determinations (Berne and Pecora, 1976).) Light passing through a medium is scattered due to regions of different refractive index, n; thus, polymer molecules dissolved in a solvent having a refractive index different from the polymer will scatter light. Ignoring the contribution from the solvent (which is small compared to the macromolecular scattering), isolated molecules (no interparticle interference) that are much smaller than the wavelength of the light (no intramolecular interferences) will scatter light with an intensity given by

$$I(q) = I_0 \left[\frac{4\pi^2 n_o^2}{\lambda^4 N_A} \left(\frac{\partial n}{\partial c} \right)_T^2 \right] Mc, \tag{3.3}$$

where q $\left(\equiv \frac{4\pi}{\lambda} \sin \left(\frac{\theta}{2} \right) \right)$ is the momentum transfer and θ is the scattering angle, I_0 is the intensity scattered through $q = 0$, λ is the wavelength, N_a is Avagadro's number, and n_0 and n are the respective solvent and solution refractive indices. The change in the refractive index with concentration is approximately equal to the ratio of the relative refractive index and the polymer mass density, $(\partial n/\partial c)_T = (n_{\text{poly}} - n_0)/\rho$. Generally, $\partial n/\partial c|_T < 0.2$ mL/g for polymer solutions.

In a given experiment, the quantity in brackets in Eq. (3.3) is a constant, K, so

$$R(q) \equiv I(q)/I_0 = KMc, \tag{3.4}$$

where $R(q)$ is the Rayleigh ratio. Polymer chains are large enough ($>\lambda/10$) that light scattered from different parts of the molecule have different phase

shifts; thus, Eq. (3.4) is modified by the molecular structure factor, $P(q)$

$$R(q) = KMcP(q). \tag{3.5}$$

This structure factor can be approximated at small scattering angles as

$$P(q) \approx 1 - \frac{1}{3}q^2 S_g^2 + \cdots, \tag{3.6}$$

which is valid for particles of any shape. S_g is the root-mean-square radius of gyration of the polymer, and small angle is defined by the condition $q \ll S_g^{-1}$. A plot of $R(q)$ versus q^2 at small q is a straight line whose intercept yields the molecular weight, and the ratio of slope to intercept yields the radius of gyration. Since the reciprocal of the Rayleigh ratio is more sensitive to small variations than R itself, Eq. (3.5) is usually rewritten (using the fact that $1 + x = [1 - x]^{-1}$ for small x)

$$\frac{Kc}{R(q)} = M^{-1}\left(1 + \frac{1}{3}q^2 S_g^2\right). \tag{3.7}$$

Thus, $R(q)^{-1}$ is plotted versus q^2, with the molecular weight and S_g obtained via extrapolation to $q = 0$.

The foregoing assumes independent scattering from each particle. At the usual polymer concentrations, even though the visual turbidity remains negligible, waves scattered from different chains interfere. This interparticle interference causes the scattering intensity to deviate from a linear dependence on c. To correct for the concentration effect, a power series expansion is assumed

$$\frac{Kc}{R(q)} = M_w^{-1}\left(1 + \frac{1}{3}q^2 \langle S_g \rangle^2\right) + 2A_2c + \cdots, \tag{3.8}$$

where A_2 is called the second virial coefficient. Note that in consideration of a distribution of molecular masses, M is now the weight average and the obtained radius of gyration is the mean-square z average. Application of Eq. (3.8) requires extrapolation to $c = 0$, in addition to the extrapolation to zero angle. These two extrapolations are carried out simultaneously via a Zimm plot (Figure 3.4). A proper Zimm plot yields both the radius of gyration and the virial coefficient, consistent with the M_w obtained for the polymer. Deviations from the linearity at lower angles indicate artifacts, such aggregates, gel, dust, and so on (Vavra et al., 1967). With rubbers, clarification problems can be especially serious due to the possibility of removing some of the polymer along with the contaminants. Using a laser beam having a small cross-sectional area, it is sometimes possible to see "between" gel or dust particles, which are then detected only intermittently as "spikes" of large scattering intensity. This may alleviate to some extent the need for solution clarification. Supplementing the data with dynamic light scattering measurements has been proposed as a means to correct for the contribution from large impurities (Lindner and Glatter, 2000).

Multiple detectors, from 3 to as many as 18, facilitate the extrapolation to zero angle. In principle, a scattering detector can be placed at a sufficiently
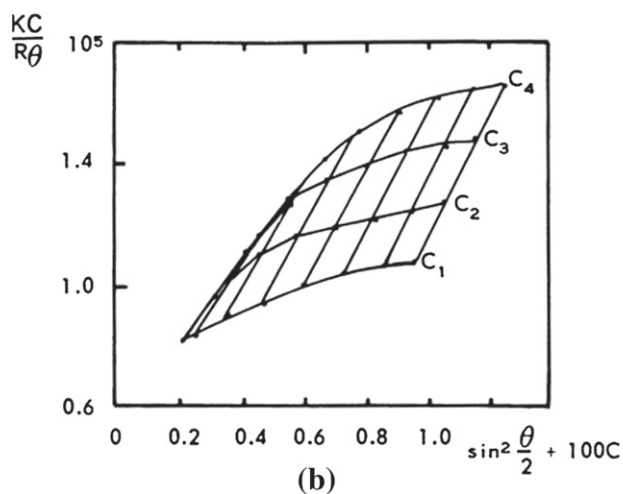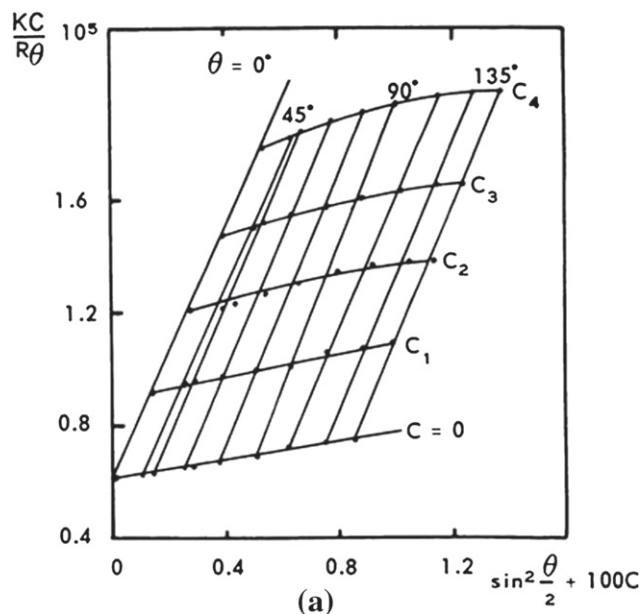
FIGURE 3.4 Zimm plots of commercial polyvinylchloride in THF: (a) purified solution with expected linear variation of $R(q)^{-1}$, (b) as received material, showing curvature due to aggregation (Vavra et al., 1967).

low angle, that such extrapolation of the scattering intensity to $q = 0$ becomes unnecessary, at least if the molecular weights are not too large. When a light scattering detector is attached to a chromatograph, the concentration of polymer is low, to some extent minifying the need for extrapolation to zero concentration. Of course, the radius of gyration and virial coefficient are not obtained. However,

in this manner, a molecular weight determination by light scattering can be completed expeditiously.

Structural information can also be obtained from measurements of small-angle neutron scattering (SANS) (Higgins and Benoit, 1997; Wignall, 1996; Lohse, 1994; Hammouda, 2010). Scattering of neutrons is due to their interaction with nuclei. It differs from light scattering, in that contrast arises from differences in neutron scattering length, rather than refractive index differences. Neutron cross-sections are commonly expressed in terms of the relevant correlation function. Elastic, coherent scattering is proportional to the spatial Fourier transform of the pair-correlation function. The angular distribution of coherent scattering is reinforced by constructive interference, and thus yields structural and conformational information. Conventional SANS probes dimensions in the range from 1 to 100 nm length scales, while so-called ultra-small angle neutron scattering (USANS) probes length scales up to tens of μm (Sharp et al., 2009). The advent of the Bonse-Hart camera, which utilizes multiple reflection crystals before and after the sample (Bonse and Hart, 1965), has overcome the historical problem of poor signal-to-noise ratios in measurements at very high resolution.

Inelastic coherent and incoherent scattering are proportional to the space and time Fourier transforms of, respectively, the pair-correlation and the self-correlation functions. Analogous to dynamic light scattering, these are used to probe polymer dynamics (Arbe et al., 2003; Richter, 2003; Stepanek et al., 2002; Annis et al., 2001).

The neutron scattering cross-sections of carbon and oxygen are completely coherent. [1]H has a very large incoherent scattering cross-section and a small coherent cross-section, while the opposite is true for deuterium. One advantage of SANS is that isotopic labeling (usually the replacement of hydrogen by deuterium) can be used to provide selective contrast. Such labeling has minimal chemical effect, enabling $\langle S_g \rangle$ and M_w to be determined in situations when light scattering cannot be used. Dust is also not a problem with SANS. An obvious disadvantage of the method is the greater cost of preparing labeled materials.

One important area in which SANS has yielded information not otherwise available is determining chain dimensions in bulk polymers. Samples can be a couple of millimeters in thickness, with up to 50% of the incident neutrons scattered. The mean-square radius of gyration and M_w can be determined for a deuterated version of a polymer mixed with its unlabeled analog. No Zimm analysis is required, despite overlap and interpenetration of the chain molecules. The only requirement is that both isotopic species have the same M_w and MWD. A model-independent analysis of the scattering used the Gunier approximation

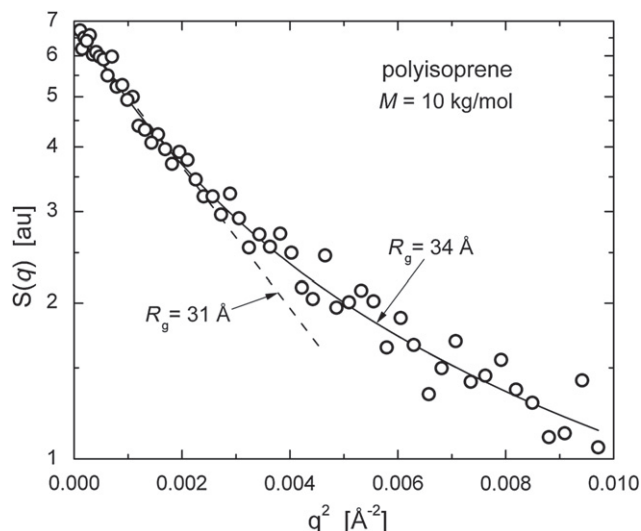$$I(q) = I_0 \exp\left(-\frac{1}{3} q^2 S_g^2\right)$$

$$(3.9)$$

FIGURE 3.5 SANS from blend of deuterated and conventional polyisoprene ($M_w = 10^4$ g/mol), plotted in the Gunier form (Eq. (3.9)) yielding a straight line at small angles. The solid line is the fit to the Debye form for Gaussian coils (Eq. (3.10)). Data from Akcasu et al. (1980).

valid at small angles. Rubber is usually comprised of flexible chains, so that the single chain structure factor is expected to have the Debye form for a Gaussian coil (Berne and Pecora, 1976):

$$P(q) = \frac{2}{q^4 R_g^4} \left[\exp\left(-q^2 R_g^2\right) - \left(1 - q^2 R_g^2\right) \right]. \tag{3.10}$$

This result is shown for polyisoprene in Figure 3.5 (Akcasu et al., 1980). Direct SANS measurements of the size of chains in the melt validated Flory's original hypothesis that polymers behave ideally in the bulk. Other applications of SANS to elastomers include investigations of microscopic aspects of network deformation (Gronski et al., 1990; Boue et al., 1991; Westermann et al., 2001) and the effect of fillers, such as carbon black and silica, on network deformation (Botti et al., 2003; Westermann et al., 1999; Zhang et al., 2001).

The two sources of neutrons are nuclear reactors and particle accelerators (spallation sources). Neutron scattering facilities in North America include the National Institute of Standards and Technology, Oak Ridge National Laboratory, the Los Alamos Neutron Science Center, Argonne National Laboratory, Chalk River (Canada) Neutron Beam Laboratory, and the University of Missouri (Columbia). Generally, access involves a proposal system for nonproprietary work, with proprietary studies on a fee basis. There are also SANS facilities in Europe, Asia, and Australia.

TABLE 3.3 Solution Viscosity Definitions ($\eta \equiv$ Solution Viscosity; $\eta_0 \equiv$ Solvent Viscosity)

Viscosity	Relative	Specific	Reduced	Inherent	Intrinsic
Definition	$\eta_{rel} = \eta/\eta_0$	$\eta_{sp} = \eta_{ret} - 1$	$\eta_{red} = \eta_{sp}/C$	$\eta_{inh} = \ln(\eta_{rel})/C$	$[\eta] = \lim\limits_{C \to 0} \eta_{red}$

In addition to the scattering methods, techniques such as cryoscopy, ebulliometry, and membrane osmometry give absolute molecular weight determinations, with the results independent of branching (Table 3.2). Methods that depend on the size of the molecule in solution, such as the intrinsic viscosity, size exclusion chromatography (SEC), sedimentation, and so on, require calibration, and the results are a function of polymer geometry, in particular long chain branching (LCB) (Table 3.2).

Another parameter that can be related to molecular weight is the relative viscosity, defined as the ratio of the viscosity of a polymer solution η to the viscosity of the solvent η_0 (see Table 3.3). Reliable for molecular weights $>10^3$ g/mol, the viscosities can be determined by measuring flow times through capillary tubes (diameters $\sim$1 mm), usually with gravity as the driving force for the flow. Automated instrumentation is widely available. Rotational and oscillatory type viscometers are used where a uniform, well-defined, or low shear rate is required. The ratio of the two viscosities, η/η_0, is called the relative viscosity, and the difference between that number and unity is the "specific" viscosity. Extrapolation to zero concentration of the specific viscosity divided by the concentration yields the intrinsic viscosity $[\eta]$. The intrinsic viscosity is related to molecular weight M as (Flory, 1969).

$$[\eta] = \Phi \langle r^2 \rangle^{3/2} / M, \tag{3.11}$$

in which $\langle r^2 \rangle$ is the mean-square end-to-end distance and Φ is a constant ($= 2.6 \times 10^{21}$ for r in cm). Equation (3.11) can be written as

$$[\eta]_\Phi = KM^{1/2}, \tag{3.12}$$

where Θ refers to Theta conditions, and $K(= \Phi(\langle r^2 \rangle/M^{3/2}))$ is constant for sufficiently high molecular weight (ca. 5000 g/mol). Working at Θ conditions is not always feasible, since the temperature control is exacting and there is a tendency for precipitation due to the limited solubility. A convenient alternative is to use the Mark-Houwink relation (Barth and Mays, 1991; Cooper, 1989; Zeng et al., 2006; Kurata and Tsunashima, 1999),

$$[\eta] = KM_v^a, \tag{3.13}$$

where $M_n < M_v < M_w$ (Figure 3.3), and a ranges from 0.5 to about 0.8 for rubbery polymers. Both K and a depend on polymer, solvent, and temperature,

and must be determined empirically using polymers of known molecular weight. For good solvents, $[\eta]$ for a polymer varies only $\pm 30\%$, and it can be estimated empirically with reasonable accuracy (Van Krevelen, 1990; Kuo et al., 1990).

A convenient and very common method of molecular weight determination ($<10^7$ g/mol) is Size Exclusion Chromatography (SEC), or the more specific term, Gel Permeation Chromatography (GPC) (Stuart, 2002; Ruckebusch et al., 2008; Dekmezian et al., 1990; Grubsic-Gallot et al., 1990; Kuo and Provder, 1987). A dilute solution of the polymer is passed through a column packed with small (e.g., 5 μm) porous articles. The pore diameters are about the size of the dissolved region polymer chains. As the polymer solution passes through the column, polymer molecules diffuse into and out of pores. The accessibility of a given pore is determined by the hydrodynamic volume of the dissolved molecules. Since small molecules fit into more pores, their elution time from the column is longer. The flow can actually be stopped for minutes with little distortion of the chromatogram. The measured parameter is the elution volume V_e, which is a function of the molecular sizes in the solution. Based on calibration under identical conditions of the column, using narrow MWD standards, the molecular weight is directly related to V_e.

Empirically, it is known that if different polymers have the same elution volume from a given GPC column, the product $[\eta]M$ will be constant, where $[\eta]$ is determined under the same conditions (T and solvent). This follows from the Einstein-Simha relation, whereby the quantity $[\eta]M$ is proportional to the hydrodynamic volume. The hydrodynamic volume depends on temperature and solvent, and is roughly half the volume calculated from S_g. Using the "universal calibration method," molecular weight determinations can be made for a polymer using known standards of a different polymer (Grubisic et al., 1967; Puskas and Hutchinson, 1993; Kuo et al., 1993). These molecular weight standards are commercially available for various polymers. From Eq. (3.13),

$$M_U = \left[\frac{K_S}{K_U} \right]^{1/(a_U+1)} M_S^{\frac{a_S+1}{a_U+1}}, \qquad (3.14)$$

where the subscripts U and S refer to the unknown and standard samples, respectively.

The resolution of a calibration curve becomes poorer at very high and low molecular weights; that is, large differences in molecular weight are reflected in small changes in elution volume. Note that additives, such as antioxidants, will also elute, so that these may be confused with a low molecular weight fraction of the polymer. Various aspects of the SEC experiment can be adjusted to improve resolution for a given determination (Barth and Mays, 1991; Cooper, 1989; Rooney and Ver Strate, 1981). The resolution is improved, *inter alia*, by smaller packing particles in the column, although this increases the potential for shear degradation of the sample. The presence of sample heterogeneity, such as blends or branching, exacerbates the resolution problem. SEC detectors include differential refractometers and UV/visible detectors,
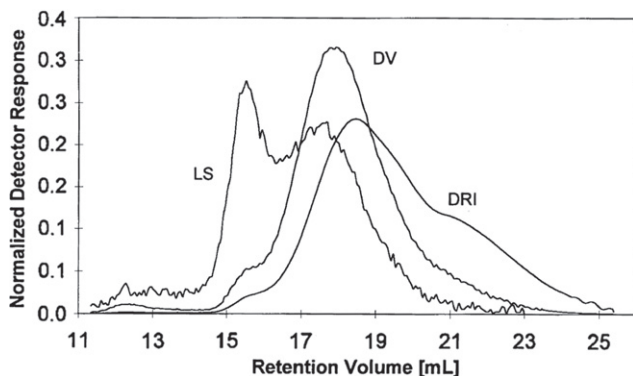
FIGURE 3.6 Chromatograms of a blend of linear and branched polyesters for light scattering (LS), viscometric (DV), and differential refractive index (DRI) detectors. The response of the LS is superior for larger molecular weights, while the DRI extends the sensitivity to larger retention volumes (Balke and Mourey, 2001).

which give a signal proportional to the polymer concentration, as well as viscometric and light scattering detectors, whose signal depends on both the concentration and the molar mass (see earlier). Multiple detectors are employed to facilitate deconvolution of overlapping retention volumes (see Figure 3.6) (Gaborieau et al., 2007; Medrano et al., 2003; Provder et al., 1995; Brun and Liq, 1998; Nagy, 2003; Wang et al., 2000; Balke and Mourey, 2001). For example, the effluent from the column passes through a light scattering cell or a viscometer, and then through a differential refractometer. The latter serves as a concentration detector, and is usually last in line, since it is most easily disrupted by downstream back pressure.

A potential error in the SEC analysis is peak broadening due to nonuniformities in the pore structure of the GPC or inherent to the flow through the column. The resolution of a column can be characterized by the ratio of the spread of the elution volume for a monodisperse sample to the peak of the retention volume. At the extremes of the range for a broad MWD sample, a given elution volume can shift by as much as 50% in molecular weight for repeat measurements on the same sample. This type of peak broadening is due to diffusion, mixing, and concentration effects, and perhaps in part to a dependence of the hydrodynamic volume on concentration. Another source of error for very high molecular weight samples (e.g., $M \sim 10^6$ g/mol or higher) is mechanical degradation (chain scission) during transport through the column (Rooney and Ver Strate, 1981).

The classical method of solvent-nonsolvent fractionation according to MWD and compositional distribution relies on solubility differences among the various species. The method is empirical and tedious, involving characterization of phase-separated "cuts." However, fractionations can be carried out with minimal equipment, and for some polymers are the only source of narrow compositional

and MWD standards for techniques such as SEC or [η]. TREF, described earlier, is an automated implementation of the fractionation procedure.

The term Field Flow Fractionation (FFF) (Barth and Mays, 1991; Cooper, 1989; Messaud et al., 2009; Williams and Lee, 2006; Lee and Molnar, 1995; Schimpf et al., 2000; Lee et al., 2000) refers to a family of one-phase chromatographic techniques, carried out in thin flow channels. In principle, FFF yields absolute molecular weights, although in practice calibrations similar to SEC are used. An external field is applied perpendicular to the laminar flow of solvent in a channel. The parabolic velocity profile of the flow causes separation according to the position of molecules with respect to the wall. Molecules having weaker interaction with the field remain further from the walls of the channel, thereby eluting sooner. The external field may be a flow field, an electric or magnetic field, or a thermal field. In Thermal Field Flow Fractionation (TFFF) (Lee and Williams, 2010; Kim et al., 2006; Stegeman et al., 1994; Lee and Molnar, 1995; Lewandowski et al., 2000) a temperature gradient of tens of degrees is imposed, causing migration and accumulation of the solute polymer at the cold wall, in competition with Brownian motion. The transport coefficient governing the thermal diffusion depends on chemical composition, as well as molecular weight. For a given solute, smaller molecules, having the larger diffusion coefficients, migrate more toward the center, and are thus eluted first by the flow. In addition to discrimination according to molecular size, TFFF can be used to measure thermal diffusion coefficients of chain molecules (vanAsten et al., 1996; Nguyen et al., 1998).

FFF is fast and provides good mass resolution. Attractive features include the absence of a substrate and the channel being too large to be plugged by gel (useful since polymer samples often contain gel). The method can be applied to molecular weights up to ca. 10^7 g/mol, and commercial instruments are available.

An absolute method for molecular weight determination is matrix-assisted laser desorption ionization time-of-flight mass spectrometry (MALDI-TOF) (Kona et al., 2005; Creel, 1993; Nielsen, 1999; Cho et al., 2001). The sample is dispersed in a UV-absorbing matrix (e.g., *trans*-cinnamic acid or 2,5-dihydroxybennzoic acid). Irradiation with a UV laser induces evaporation of ionized polymer chains, which are then detected using TOF. The technique requires relatively narrow MWD samples. Alternative ionization methods have been employed, such as electrospray ionization mass spectrometry (ESI-MS), which may have advantages for certain polymer end groups (Vana et al., 2002). TFFF and MALDI-TOF can be coupled to analyze polydisperse samples and polymer mixtures (Kassalainen and Williams, 2003).

Sedimentation relies on gravity to drive the separation of macromolecules according to their size, with high rotation speeds (up to 70,000 rpm) used to accelerate the process (Stuart, 2002). Ultracentrifugation (Scott et al., 2005; Laue, 1990) emerged as a versatile, powerful method with the development of new detection methods, based on Schlieren optics, UV/VIS absorption,

Rayleigh interference, fluorescence, light scattering, turbidity, and multiwavelength UV/VIS optics (Karabudak et al., 2010). It is widely applied to the analysis of proteins, providing the ability to examine the quaternary structural state, as well as conformational changes (Chou et al., 2011; Schuck, 2000). Nonequilibrium, sedimentation velocity measurements are employed, which are quicker but less rigorous than equilibrium experiments. Ultracentrifugation is one of few techniques yielding the z-average molecular weight, and it can also provide information concerning sample homogeneity.

The methods discussed heretofore involve polymer solutions. Neat samples are analyzed directly via melt viscosity measurements. At shear rates lower compared to the rate of Brownian motion of the chains, the melt viscosity is independent of shear rate (Newtonian behavior), $\eta = \eta_0$. Thus, the viscosity-M_w relationship for a particular temperature can provide an accurate M_w determination (see Figure 3.7; Colby et al., 1987; Abdel-Goad et al., 2004). Given the high molecular weight of elastomers, the main difficulty is attaining zero-shear-rate conditions. At ambient temperatures, $\eta_0 > 10^7$ Pa s. Note that "cold flow" of unvulcanized rubber usually requires weeks or longer. The obvious way to reduce the viscosity is to make measurements at elevated temperatures. However, especially for unsaturated rubbers, degradation may occur before steady-state conditions can be attained. The situation is worse if the polymer has long chain branching.
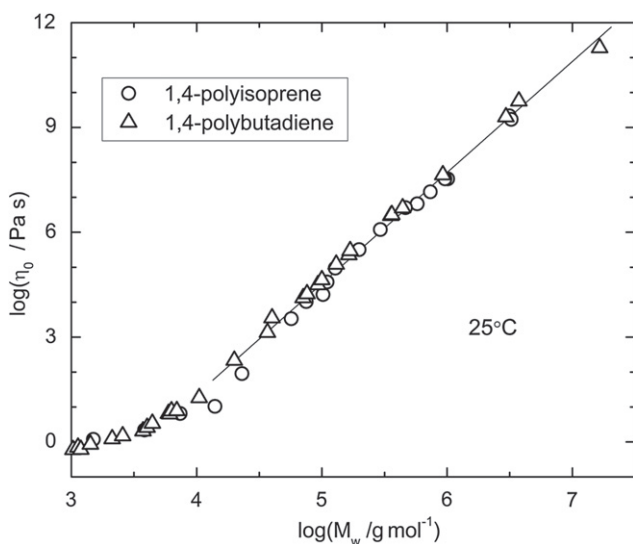

FIGURE 3.7 Zero-shear-rate viscosities of 1,4-polybutadiene (Colby et al., 1987) and 1,4-polyisoprene (Abdel-Goad et al., 2004). The line is the best-fit to molecular weights at least three times the entanglement molecules (= 1850 and 6190 for PB and PI, respectively), which gives a power-law slope equal to 3.2.

3.4.2 Branching

Side-chains on a polymer backbone are described as either short-chain branching (SCB) or long-chain branching (LCB), the latter defined as branches having molecular weights at least a few times the entanglement molecular weight. Branching affects various properties, for example the geometry and size of the chain molecule (Figure 3.8), affording means to characterize the degree of branching (Grest et al., 1996).

The intrinsic viscosity is reduced by LCB (viz. Eq. (3.10)), with a smaller ratio of the respective mean-square radii of gyration of branched and unbranched polymers having the same M_w:

$$g = \frac{\langle S^2 \rangle_{\text{br}}}{\langle S^2 \rangle_{\text{lin}}}, \quad g' = \frac{[\eta]_{\text{br}}}{[\eta]_{\text{lin}}}. \tag{3.15}$$

The parameter g is less than unity for polymers with LCB, and sometimes defined as the ratio of the root-mean-square values, $S_{g,\text{br}}/S_{g,\text{lin}}$. The calculation of g for a given branch structure is straightforward, but radii of gyration are hard to measure experimentally. Intrinsic viscosities are readily measurable, but relating g' to g, and thus to branch structure is difficult. Calculations of g' involve dilute solution theory, as discussed following Eq. (3.10), with the
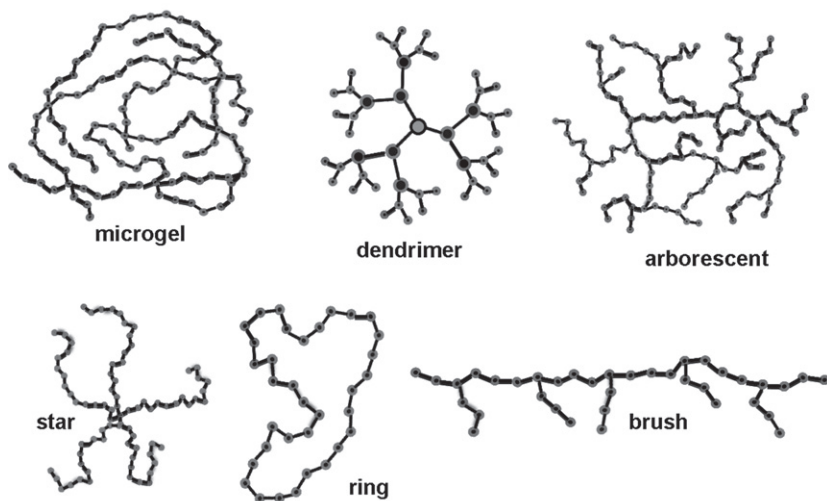

FIGURE 3.8 Chain architectures: Microgel formed by polymerization and crosslinking of monomers dispersed as an emulsion; dendrimer formed by cascade synthesis to yield (in this example) a third-generation tiered polymer; arborescent branched polymer, which lacks the regularity of a dendrimer; star polymer, in which each arm originates from the same unit and terminates in a dangling end; ring or cyclic polymer; brush or comb polymer, in which dangling chains are anchored to a linear backbone (Roland, 2011).

type of branching explicitly considered. Alternatively, g may be evaluated using model polymers. Determination of absolute levels of branching from intrinsic viscosity measurements is not possible, since it depends on the nature of the branching, including the junction functionality and branch architecture (random, star-branched, dendrimeric, etc.). However, relative values of g' can be used to assess relative degree of branching.

With light scattering measurement of the radius of gyration (see Eq. (3.6)), direct comparisons of g values can be made. In Θ solvents, the experimental g values generally agree with calculations, with some exceptions (Small, 1975).

SEC can be used to detect branching (Zheng et al., 2011, 2012a,b; Zhang et al., 2012; Ponomarenko et al., 2012; Puskas et al., 2012; Suarez and Coto, 2011; Samperi et al., 2011; Castignolles and Gaborieau, 2010; Minari et al., 2010). Since the product $M[\eta]$ is constant for a fixed value of the SEC elution volume, SEC data can be obtained for a homogeneous fraction of a sample of unknown branching, and the ratio of its intrinsic viscosity to $[\eta]$ of the linear polymer having the same elution volume is calculated. This M calculated from its intrinsic viscosity is then compared to the molecular weight of the unknown determined by an absolute technique.

An empirical relationship for broad MWD samples gives an average value

$$g'' = \frac{M_{v,\text{lin}}}{M_{w,LS}} \times \left(\frac{M_w}{M_v}\right)_{\text{GPC}}, \tag{3.16}$$

in which $M_{v,\text{lin}}$ is the molecular weight calculated from the intrinsic viscosity assuming the polymer is linear, $M_{w,LS}$ is from light scattering measurements, and $\left(\frac{M_w}{M_v}\right)$ is taken from the elution volumes assuming no branching. As an example, for NBS 1476 (a polyethylene standard with LCB), $g'' = 0.4$, using $[\eta] = 1.04$ dl/g in decalin, $(M_w/M_v)_{\text{SEC}} = 1.16$, $M_{w,LS} = 125,000$ g/mol. The number of branches yielding this value of the branching parameter depends on the nature of branching. For random tetrafunctional branches, $g = 0.4$ corresponds to 20 chain ends per weight average chain.

Advanced SEC analytical techniques take advantage of online light scattering and viscometry [III B 4-10]. With the SEC calibrated for the product $[\eta]M$ versus elution time for a particular polymer species, together with $[\eta]_{\text{Br}}$ or M_w^{Br} measurements, g factors can be calculated as the ratio of the measured intrinsic viscosity to the value calculated for the corresponding linear polymer (i.e., the linear polymer that would have eluted at the same time).

If well-characterized samples are available, a calibration of viscoelastic properties for the neat material, such as the melt viscosity, can be used to assess LCB. Below a certain molecular weight (which is a few times the entanglement molecular weight), branching reduces the melt viscosity, since the molecular size is smaller for fixed molecular weight. Since LCB inhibits motion along the chain contour (reptation), it can effect an enormous increase in the viscosity

and terminal relaxation times. A polymer with LCB is always more viscous than its linear counterpart of equal M_w (Grest et al., 1996; Kraus and Gruver, 1965; Ngai and Roland, 1997; Robertson et al., 2001), and for this reason LCB is introduced by design in some commercial rubbers to reduce cold flow (i.e., the room temperature creep of rubber during storage). Substantial LCB may require use of a polymer with a low number-average molecular weight, in order to retain a viscosity low enough for processing; however, the consequent high concentration of chain ends may be deleterious to cured properties, for example heat buildup or strength.

For rubbers such as NR (or synthetic 1,4-polyisoprene) (Santangelo and Roland, 1998) and polybutadiene (both 1,2- and 1,4-isomers) (Carella et al., 1986), LCB increases the temperature sensitivity of the viscosity and terminal relaxation time. Thus, by comparing apparent activation energies, or, in the more usual case where the behavior is non-Arrhenius, the temperature dependence of the ratio of relaxation times for an unknown and a linear sample of the same polymer, inferences can be drawn concerning LCB (Figure 3.9). For polymers such as 1,4-polyisoprene, which have a dipole moment parallel to the chain, dielectric measurements of the normal mode can be used to measure the temperature dependence and thus assess the presence of LCB.

Note that LCB does not enhance the T dependence of all rubbers. For example, the temperature dependence is the same for linear and branched polyisobutylene (Robertson et al., 2001; Santangelo et al., 1999), polydimethysiloxane (Roland and Santangelo, 2002), and hydrogenated 1,2-polybutadiene (Carella et al., 1986).

Although short branches do not suppress reptation and thus have a weak effect on the rheology, SCB can alter many physical properties, indirectly through suppression of crystallization and directly by changing the shape and flexibility of the chain molecules. The degree of SCB can be measured by NMR (Feast et al., 1997) and FTIR (Blitz and McFaddin, 1994). A high concentration of SCB increases the spatial extent of the chain, to reduce steric congestion of the side-groups with themselves and with the repeat units of the backbone. Thus, polymers with substantial SCB are less flexible. A measure of this property is the persistence length, l_p, defined as the distance over which bond orientations become uncorrelated. For a freely jointed chain l_p equals one bond length, while for a completely rigid rod polymer, the persistence length just equals the chain length. An empirical equation relating l_p to the number branches is (Ramachandran et al., 2008)

$$l_p = l_p^\infty - a_{\text{SCB}} \exp\left(-n/b_{\text{SCB}}\right) \qquad (3.17)$$

in which l_p^∞ is the persistence length for complete branching, and a_{SCB} and b_{SCB} are constants, the former specific to the polymer chain and the latter depending on the type of branches.
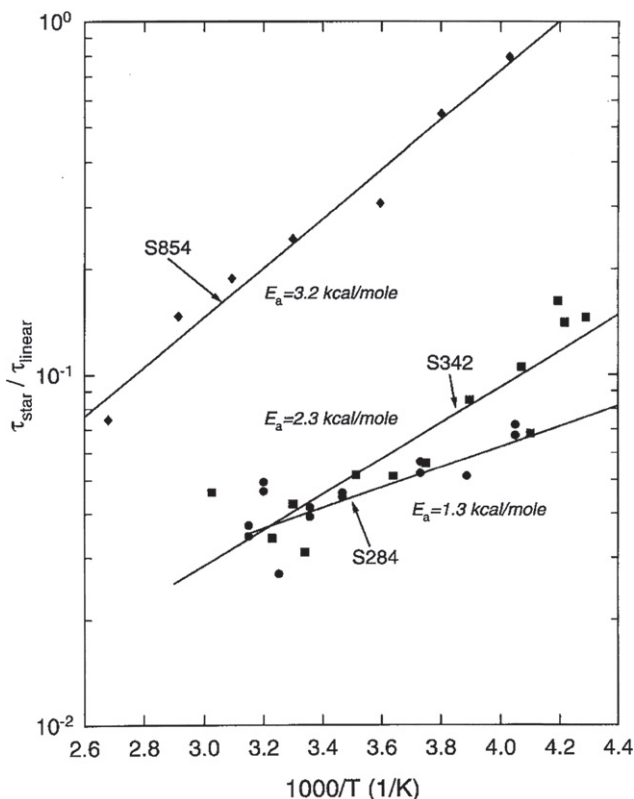
FIGURE 3.9 Terminal relaxation times of 3-arm star 1,4-polyisoprenes having M_w (g/mol) = 284,000 (S284), 342,000 (S342), and 854,000 (S854), normalized by the relaxation time for linear 1,4-polyisoprene. The excess activation energy due to the LCB is ~400 J per mole of branch entanglements. (Reprinted from Santangelo and Roland, 1998).

Ramachandran et al. (2011) used Eq. (3.9) to obtain average coil size and a power-law to describe the rod-like character at high q

$$I(q) = B_f q^{-d_f}. \tag{3.18}$$

B_f is a constant prefactor and the exponent d_f represents the dimension of the fractal object; typically it is assumed $d_f = 1$. From fits to SANS scattering data the persistence length can be extracted. Figure 3.10 (Ramachandran et al., 2011, 2008) shows the results for the stiffening of the polyethylene due to the presence of short-chain branches.

3.4.3 Gel

The presence of gel suppresses flow of a rubber. In gel-sol studies crosslinks are introduced in a controlled fashion (e.g., using peroxide or ionizing radiation), and the initial molecular weight is determined from the gel dose. The analysis,
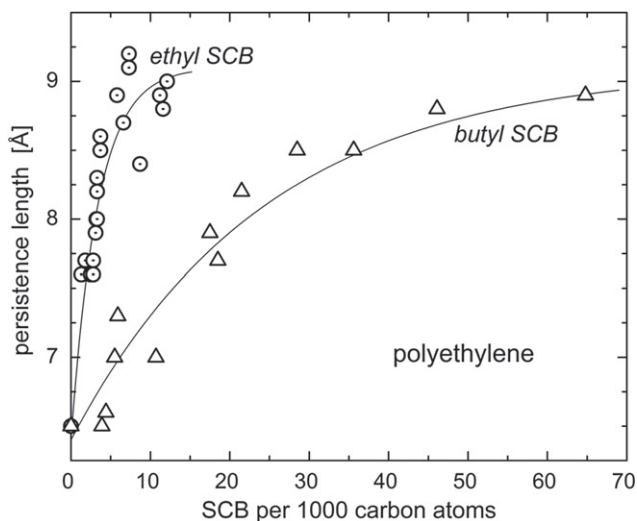
FIGURE 3.10   Persistence length of polyethylene from SANS versus the number of ethyl (circles) (Ramachandran et al., 2011) or butyl (triangles) (Ramachandran et al., 2008) short-chain branches per 1000 carbon atoms. The solid lines are fits to Eq. (3.17) with $l_p^\infty = 9.1$ Å, $a_{SCB} = 2.7$, and $b_{SCB} = 3.4$ and 24.6, respectively, for ethyl and butyl SCB.
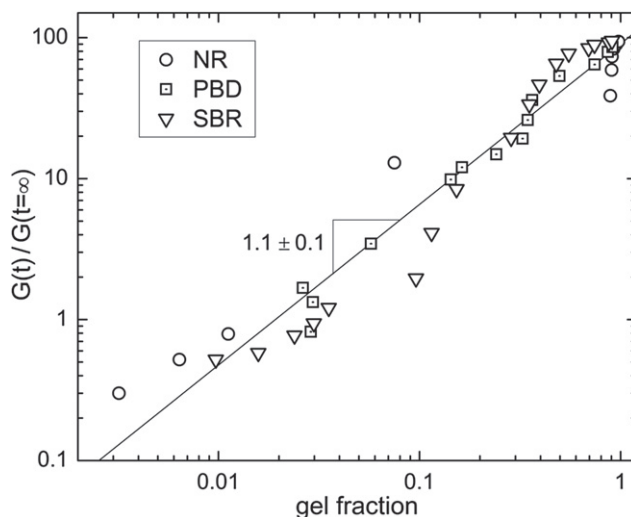

FIGURE 3.11   Rheometer torque normalized by the fully cured plateau value versus the gel content during sulfur vulcanization of three rubbers (Zhang et al., 2010).

however, requires knowledge of the rates of both crosslinking and chain scission. As crosslinking proceeds beyond the gel point, the partition between gel and sol is governed by the MWD of the sample, which in principle can be used to measure MWD (Bohm and Tveekrem, 1982).

Networks with crosslink densities only slightly beyond the gel point have minimal mechanical strength. Thus, care must be taken in dissolution of the soluble fraction to avoid damaging the network. If the gel fraction data extrapolate to a negative amount of crosslinking for gelation, the implication is that the original material contained gel. Although a gelled polymer cannot flow, large stresses imposed during milling or mixing induce nonuniform flow of a lightly crosslinked rubber; the latter also have measurable Mooney viscosities. During curing the gel content continually increases, but values approaching 100% are attained only after the rheometer torque attains a plateau value (Figure 3.11 (Zhang et al., 2010)). Polymers dissolved in a solvent can associate to yield aggregated networks (Okabe et al., 1992; Horsky and Bohdanecky, 1990). This phenomenon is common with polymers that crystallize (e.g., EPDM, polyvinylchloride, polyurethanes). Such reversible gelation depends on the solvent and temperature.

3.5 GLASS TRANSITION AND SECONDARY RELAXATION PROCESSES

When a measurement of polymer dynamics is made using one of a number of probes of relaxation (for example, mechanical or dielectric spectroscopy, light or neutron scattering), a maximum in the susceptibility, corresponding to maximum absorption, is observed at a frequency equivalent to that for the relevant molecular or segmental motions. Thus, in the limit of small perturbations, for which the material response is linear, the relaxation directly reflects the equilibrium Brownian motion. This follows from fluctuation-dissipation theory, originally proposed to explain Johnson noise in electrical conductors (Roland, 2011). The gigantic size of polymer molecules provides for an enormous number of degrees of freedom, and thereby motion encompassing many decades of time over a broad range of length scales (see Figure 3.12). The longest relaxation processes involve transport of the chain center of mass, and these are termed the terminal dynamics. At shorter times, relaxation involves motion of progressively smaller portions of the chain molecule. The rubbery plateau reflects the transient entanglement network, whose dissolution gives rise to a peak in the loss modulus (and in the dielectric loss for polymers having a dipole moment parallel to the chain (Runt and Fitzgerald, 1997; Kremer and Schonhals, 2003)). At frequencies beyond the rubbery plateau, chain motions are unaffected by entanglements. In the softening zone, the modulus is a strong function of frequency, with the behavior referred to as Rouse dynamics. (The Rouse theory was originally developed for dilute polymer solutions, but with small modification can be applied to unentangled polymer melts (Roland, 2011).) Near the end of the transition zone, the portion of a chain involved in the relaxation is too short for Gaussian behavior (that is, its end-to-end distance does not have a Gaussian distribution). These "sub-Rouse modes" (Ngai and
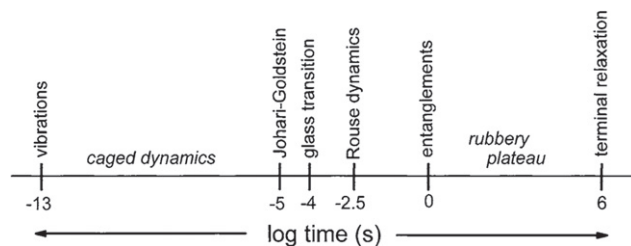
FIGURE 3.12 Schematic indicating range of motions and corresponding frequencies for 1,4-polyisoprene ($M_w = 500,00$ g/mol) at $-40\,^{\circ}C$.

Plazek, 1995) become the local segmental dynamics at the highest frequencies prior to the onset of glassy behavior.

The local segmental dynamics are associated with the rubber-to-glass transition that occurs close to T_g. Only in the glass transition zone of the viscoelastic spectrum are the chain modes and local segmental modes close enough in frequency to be measured simultaneously with conventional spectroscopies. Since the chain modes and the local segmental dynamics have different temperature dependences (Santangelo and Roland, 1998; Plazek et al., 1995; Roland et al., 2001), their mutual contribution to the viscoelastic response causes a breakdown of the time-temperature superposition principle in the glass transition zone. Thus, although master curves for the chain dynamics can be constructed that extend from the end of the softening zone through the terminal relaxation, and master curves of the local dynamics are possible, within the softening zone, the shape of the viscoelastic spectrum changes with temperature (see Figure 3.13).

While all relaxation times depend on temperature and pressure, only the global motions (viscosity, terminal relaxation time, steady-state recoverable compliance) are functions of M_w (and to a lesser extent MWD). The glass transition temperature of rubbers is independent of molecular weight because chain ends for high polymers are too sparse to affect this bulk property (Figure 3.14; Bogoslovov et al., 2010). The behavior can be described by the empirical Fox-Flory equation (Fox and Flory, 1954):

$$T_g = T_{g,\infty} - k_{FF}/M_n. \tag{3.19}$$

Note the use of the number-average molecular weight in Eq. (3.19), since it is a measure of the concentration of chain ends.

At frequencies faster than for segmental relaxation, or at temperatures below T_g, secondary relaxation process can be observed, especially in dielectric spectra. In polymers, many of these secondary processes involve motion of pendant groups. However, the slowest secondary relaxation, referred to as the Johari-Goldstein process (Ngai and Paluch, 2004), involves all atoms in the repeat unit (or the entire molecule for low M_w materials). This process is referred to as the Johari-Goldstein relaxation, and it serves as the precursor to the prominent glass transition.
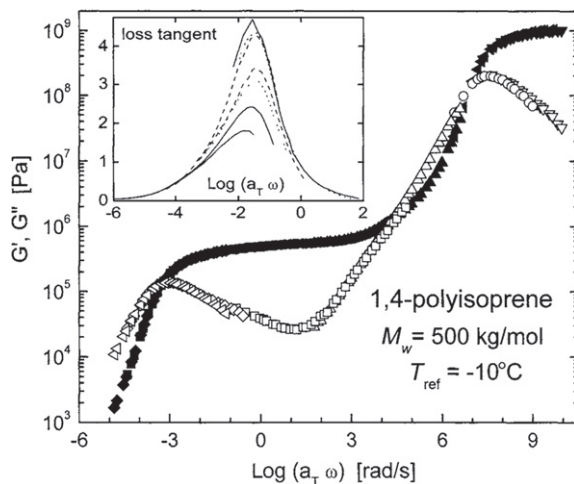
FIGURE 3.13 Apparent master curves (reference temperature $= -10\,°C$) for the storage (solid symbols) and loss (hollow symbols) moduli of cis-1,4-polyisoprene ($M_w = 500,000$ g/mol). The breakdown of time-temperature superpositioning, barely evident in the softening zone, is seen clearly in the loss tangent peak, which is shown in the inset for temperatures from $-66\,°C$ to $-48\,°C$ (the peak height decreases with increasing temperature) (Santangelo and Roland, 1998).
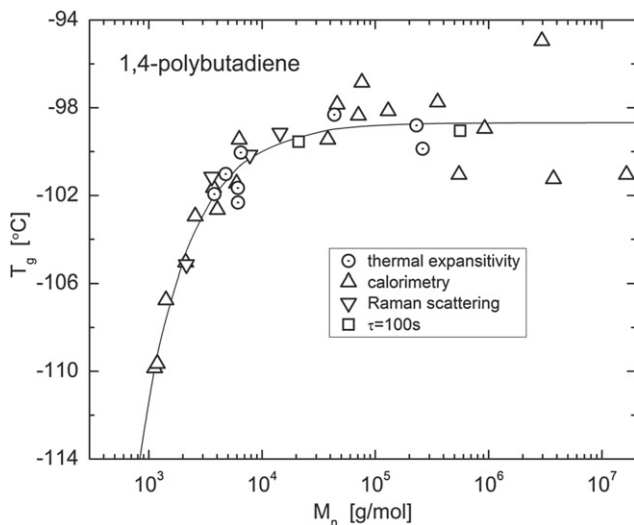

FIGURE 3.14 Glass transition temperatures measured by the change in thermal expansion coefficient (circles), from calorimetry (triangles), by Raman scattering (inverted triangles), and by relaxation spectroscopy for $\tau_\alpha = 100$ (square). The solid line is the fit to the Fox-Flory equation with $k_{FF} = 12$ kg/mol and $T_{g,\infty} = 174.4$K (Bogoslovov et al., 2010).
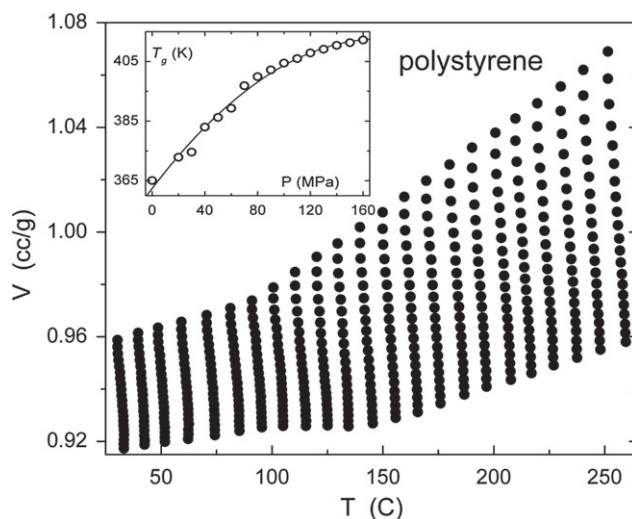
FIGURE 3.15   Specific volume of polystyrene (M_w=110,000 g/mol) as a function of temperature at various pressures. The inset shows the variation of T_g with pressure (Roland and Casalini, 2003).

The T_g of an elastomer is below room temperature, and for conventional applications it is usually lower than $-30\ °C$; otherwise, at ambient temperature, the material would lack the flexibility associated with rubbery behavior and be overly sensitive to temperature fluctuations. The glass transition is a second-order transition because, unlike melting or boiling, there is no discontinuity in the volume or heat capacity at T_g, but only a discontinuous change in the rate of change (i.e., in the thermal expansion coefficient and specific heat) (Figure 3.15) (Roland and Casalini, 2003). Experimentally, T_g simply reflects the temperature at which local segmental motions become slow relative to the experimental timescale. This means that values of T_g are a function of both the measurement frequency and, to a lesser extent, the particular relaxation process under observation. There exists a host of properties that can serve as indicators of T_g (Figure 3.14). A common one is the softening point; however, changes in stiffness of a material can reflect melting of crystalline domains, rather than a transition from the glassy state. T_g is affected by the presence of co-monomers in the chain backbone, similar to the behavior of miscible blends, and by nonpolymeric ingredients in the formulation. Both plasticization (lowering of T_g) and anti-plasticization (increase of T_g) can be brought about by addition of lower and higher T_g components, respectively.

In experiments in which temperature is scanned to determine T_g, the measurement frequency is approximately the ratio of the rate at which T is changed to the transition temperature. In such nonisothermal measurements, it

is preferable to approach T_g from the equilibrium state (i.e., by cooling), since the properties in the glassy state change due to physical aging. Physical aging refers to structural relaxation below T_g, associated with the slow decrease of the density to its equilibrium value. This causes changes in physical properties, including a shift of the glass transition temperature. A metric of the degree of nonequilibrium is the fictive temperature, T_f, also referred to as the structural temperature. T_f is the temperature at which the enthalpy of the material would be the equilibrium value.

The most common means to assess T_g is via heat capacity (C_p) measurements, usually carried out in differential scanning calorimeters (DSC). The temperature of the sample is changed at a fixed rate, with the heat flow monitored. An older and largely obsolete variation is differential thermal analysis (DTA), in which heat flow is programmed, and the consequent rate of temperature change is measured. With either method, a discontinuity in the response evidences a thermal transition. In a DSC experiment, T_g is usually taken to be the midpoint of the change in heat capacity; alternatively, T_g can be defined as the temperature of the intersection of the extrapolated baseline with the tangent of the maximum slope (Sircar, 1997). If the polymer chain is envisioned as a string of flexible beads, the head capacity change at T_g, which is almost entirely configurational, is about 11 J/K per mole of beads (Wunderlich, 2007). When DSC measurements are made during heating, the sample begins in a nonequilibrium state; thus, physical aging during the measurement can cause an endothermic peak to appear at the onset of the glass transition. In this situation, the fictive temperature is more informative than the apparent transition temperature. A graphical method for determining T_f is illustrated in Figure 3.16.

In modulated (or alternating) DSC (MDSC) (Hutchinson, 2003; Hohne et al., 2002; Simon, 2001; Pielichowski and Flejtuch, 2002), an oscillating heating (or cooling) rate is superimposed on the usual linear temperature ramp. There are two principal ways to interpret the data: obtain the complex heat capacity and decompose into the real (stored) and imaginary (dissipated) heat capacity, or separate the measured heat flow into reversing and nonreversing components (Schawe, 1995). In either method the objective is to distinguish time-independent effects from kinetic processes. MDSC is useful for studying transitions too weak to be detected by conventional DSC, analysis of multiple endotherms, and separating preexisting crystallinity in the sample from that occurring during the DSC measurement. A development in MDSC (or differential calorimetry) is the quasi-isothermal method, in which a temperature oscillation is applied without any temperature ramp, and the procedure is repeated for a range of fixed temperatures. (This is the usual method of performing isothermal dynamic mechanical and dielectric relaxation spectroscopies.) The reversing heat capacity is obtained from the measurements, with the total heat capacity determined by a conventional DSC experiment. Quasi-isothermal MDSC is used to study crystallization in polymers (Cebe, 2005) and can also provide accurate absolute heat capacities (Krishnan and Nagarajan, 2010).
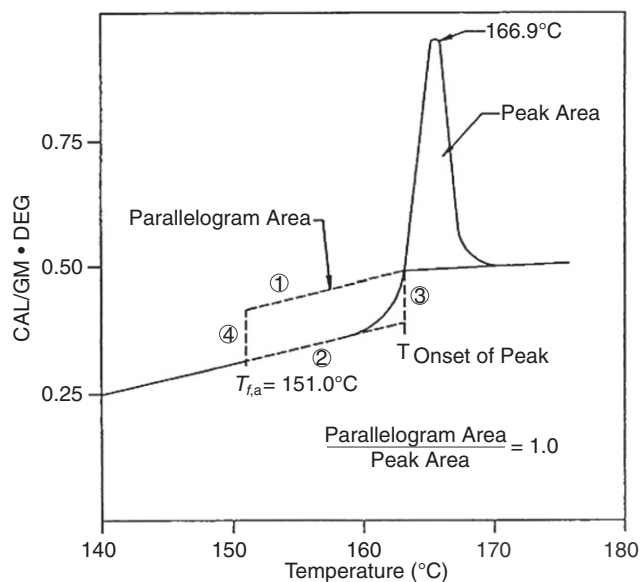
FIGURE 3.16   DSC of a cured epoxy resin. To determine the fictive temperature, a parallelogram is constructed to the low temperature side of the enthalpy peak, with horizontal sides parallel to the measured heat capacity. The onset of the peak defines the high temperature boundary, and the low temperature boundary (i.e., T_f) is chosen such that the area of the parallelogram equals the peak area.

A recent development in thermal analysis that has been applied to polymers is nanocalorimetry, in which a chip with one or two sensors is used to make heat capacity measurements on thin films (Mileva et al., 2009; Mathot et al., 2011). Sample masses of a few tens of nanograms can be analyzed, with sensitivities of picoJoule per K. Because of the small thermal mass, temperature ramps as high as 10^4 K/s can be achieved.

3.6 MORPHOLOGY

Analysis of the morphology of an elastomer includes not only characterizing the molecular structure of the polymer and of the compounding ingredients, but may also extend to the supermolecular scale: the filler network structure (see Chapter 8), the phase morphology in heterogeneous blends and thermoplastic elastomers, and any aggregates (clusters) in rubbers, for example, containing ionic groups (e.g., carboxylated rubber). A survey of experimental techniques is given in Figure 3.17. Selected aspects of rubber morphology are discussed in the following sections.

3.6.1 Orientation

Rubber elasticity arises from the orientation of chain segments, and the degree of this orientation underlies the mechanical properties. The most facile way to
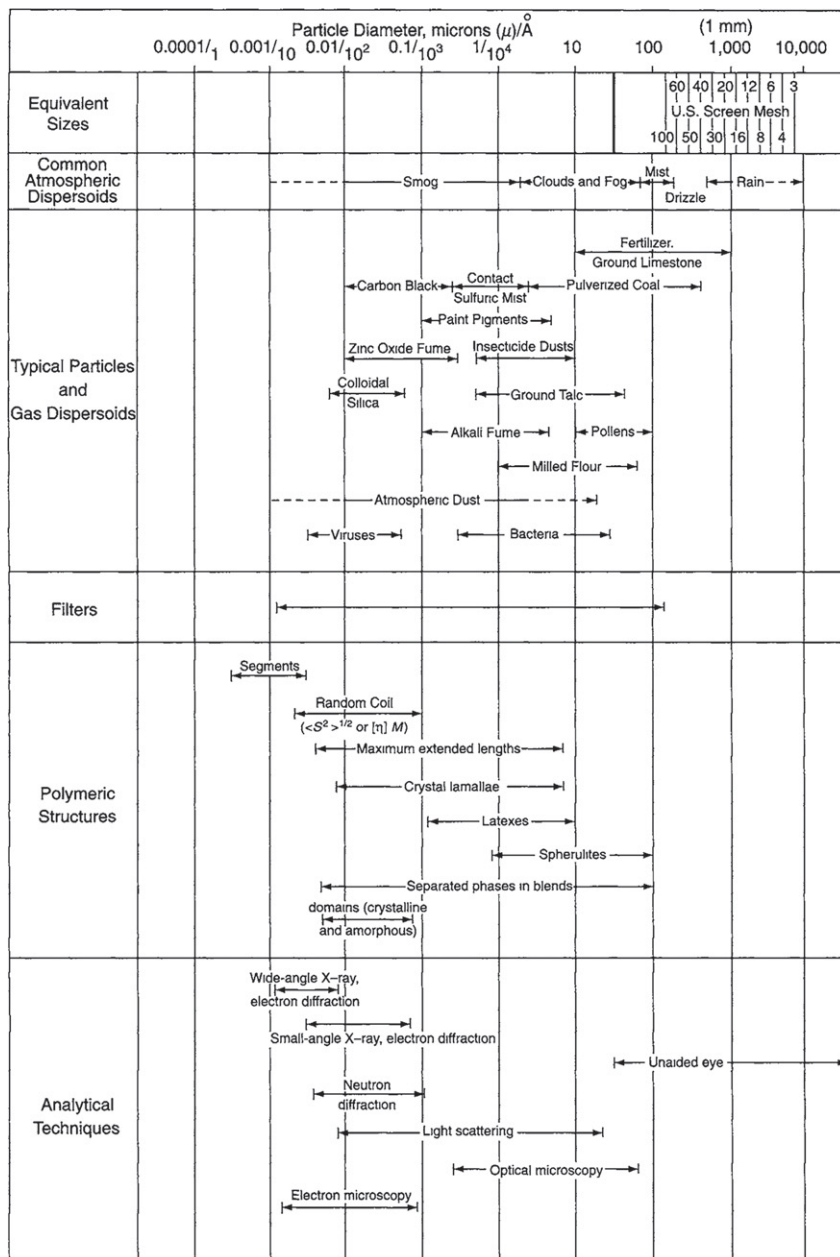
FIGURE 3.17   Characterization of particles.

quantify the orientation is from the (optical) birefringence, defined as the difference in refractive indices for two perpendicular directions. This birefringence depends on the optical anisotropy of the chain units and their degree of orientation. The mechanical stress is proportional to this same orientation factor; namely, the stress optical rule in Chapter 6.

In a semicrystalline material the observed birefringence is the sum of the Δn from the oriented amorphous phase and from the crystalline regions, which provides the measurement as a means to quantify the crystallinity in polymers. However, the contribution from form birefringence, due to the distortion of light waves traversing the boundary between the amorphous and crystalline phases (or any phases with different refractive indices), can cause the degree of crystallinity to be overestimated.

Another method of measuring polymer orientation is infrared dichroism, which refers to the ratio of the IR absorption for light having orthogonal polarizations. IR dichroism yields the same information as birefringence measurements (i.e., the second Legendre polynomial, $f_2(\phi)$), but with the advantage of chemical selectivity. The orientation of specific groups can be determined, as well as the orientation of the components in mixture (Zemel and Roland, 1992a; Myers and Cooper, 1994; Everall and Bibby, 1997; Bruell et al., 2010). Analysis requires knowledge of the orientation of the vibrational transition moment with respect to the chain axis. A few percent of deuterated polymer can be added to the sample, so that the infrared measurements can be carried out on thick samples, while still conforming to Beer's law (absorbance < ca. 0.7). Thicker samples also enable simultaneous measurement of the stress (Kannan and Kornfield, 1994). The complementary technique, polarized Raman spectroscopy, is also used to characterize orientation (Jiang et al., 2008; Park et al., 2011; Bower et al., 1995).

In polarized fluorescence measurements, the sample is illuminated by polarized light, with the emitted intensity measured for polarization parallel and perpendicular to the excitation radiation (Bur et al., 2000; Hennecke et al., 1992). A probe dye can be added to enhance sensitivity. The experiment yields both $f_2(\phi)$ and the fourth Legendre polynomial,

$$f_4(\phi) = \langle 35\cos^4\phi - 30\cos^2\phi + 3\rangle/8.$$

The latter is a more strongly decreasing function of ϕ than is $f_2(\phi)$, so that $f_4(\phi)$ reflects the more oriented chains in the distribution of orientations. For uniaxial strain, these two functions alone are adequate to describe the orientation (Bower, 1981).

Another method to characterize orientation is deuterium NMR (Dupres et al., 2009; Ekanayake et al., 2000; Valic et al., 2003). Deuterons have a spin quantum number equal to 1, and therefore a nuclear quadrupole moment. Coupling between the quadrupole moment and the two possible NMR transitions

(resulting from the three Zeeman levels of the spin $= 1$ nucleus) yields differences in the energy levels of the two transitions, giving rise to a doublet. The separation in this doublet is proportional to $f_2(\phi)$ (which depends on the orientation of the chemical bond axis of the deuteron to the applied external magnetic field); thus, the magnitude of the observed splitting yields directly the orientation.

Orientation in crosslinked elastomers primarily reflects the configurational entropy and intramolecular conformational energy of the chains. However, as first shown by deuterium NMR experiments on silicone rubber (Deloche and Samulski, 1981; Sotta et al., 1987), unattached probe molecules and chains become oriented by virtue of their presence in a deformed network. This "nematic coupling" effect is brought about intermolecular interactions (excluded volume interactions and anisotropic forces) which can cause "nematic coupling" (Zemel and Roland, 1992a; Tassin et al., 1990). The orientation is only locally effective, so it makes a negligible contribution to the stress (Doi and Watanabe, 1991), and the chains retain their isotropic dimensions (Sotta et al., 1987).

Wide-angle X-ray scattering can be used to evaluate orientation, but it is more suited to semicrystalline polymers. In principle, scattering methods can yield all orientation functions, although experimental limitations restrict determinations to $f_4(\phi)$. Using high flux synchrotron X-ray sources, transient orientations can be measured. This has been used to study the behavior of the amorphous phase during stretching of NR (Figure 3.18; Toki et al., 2003, 2011).

3.6.2 Blends

Although many rubbers can be mixed to form a blend that is homogeneous, the overwhelming majority of such mixtures are phase-separated on the microscopic scale. This does not mean the latter are not useful, since the only requirements are that a satisfactory dispersion is obtained and there is sufficient compatibility to avoid macroscopic demixing of the components. Thermodynamic miscibility, which implies segmental mixing of the components, is rare, although a number of thermodynamically miscible elastomer blends are known. The phase size in a heterogeneous blend will depend on the compatibility of the components, the relative viscosities of the components, and the mixing conditions (Roland and Bohm, 1984; Avgeropoulos et al., 1976; Paul and Barlow, 1980; Peng et al., 2011; Sirisinha et al., 2003; Chen et al., 2006). The particle size distribution can be determined from electron micrographs, using image analysis software (Cheng and Nauman, 2004; Qu et al., 2004). If the image contrast is poor, some underestimation of domain sizes can result, due to poorly discerned peripheries. In microtomed samples, errors can arise if the section thickness is less than the particle size (Weibel, 1973).

In principle, the dispersed phase size distribution can be determined from small-angle scattering experiments, using either X-rays or neutrons. Since a comparatively large volume is sampled by the incident beam, scattering
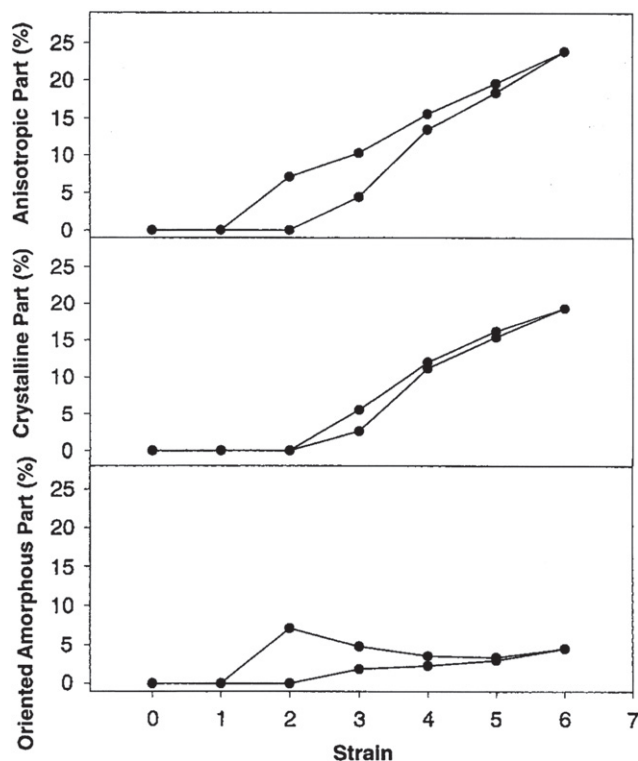
FIGURE 3.18 Total anisotropic fraction, crystal fraction, and oriented amorphous fraction of sulfur vulcanized NR stretched slowly at ambient temperature. The upper points correspond to extension, and the lower to retraction. For strains >200%, crystallization is induced, resulting in a decrease in the amorphous phase orientation.

methods are less subject to bias than micrographs. However, an inherent problem in obtaining structural information from scattering experiments is that only a limited range of reciprocal space is probed, although this limitation has been largely overcome with the advent of USANS (Sharp et al., 2009). The size distribution cannot be uniquely determined from a scattering curve. Only "scattering equivalent" distributions are obtained, based on assumptions about the particle shape and the functional form of the distribution. In Figure 3.19 the dispersed particle size of 1,4-polybutadiene in polychloroprene is shown, as determined by transmission electron microscopy (TEM) and small-angle scattering measurements (Roland and Bohm, 1984). Scanning transmission X-ray microscopy, based on the chemical specificity of near edge X-ray absorption, has potential for investigating heterogeneous morphologies, although it requires a synchrotron source (Winesett et al., 2003). Figure 3.20 demonstrates its utility for resolving blend morphologies without the requirement for staining.
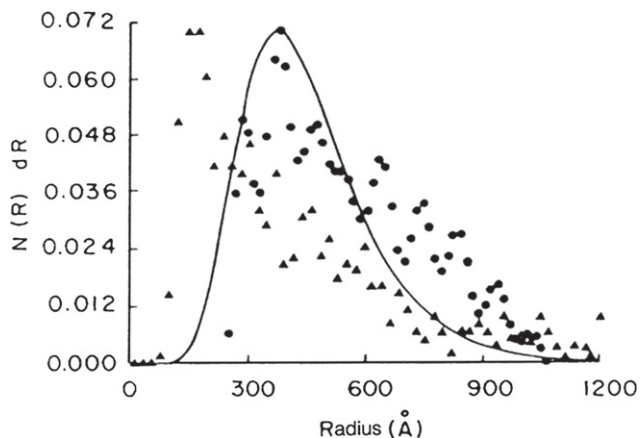
FIGURE 3.19   Size of dispersed phase in blend of 5% 1,4-polybutadiene in polychloroprene, as determined by analysis of TEM images (triangles), numerical transformation of combined SANS and SAXS data (circles), and best-fit to scattering curves assuming log normal distribution for particle sizes (solid line) (Roland and Bohm, 1984).
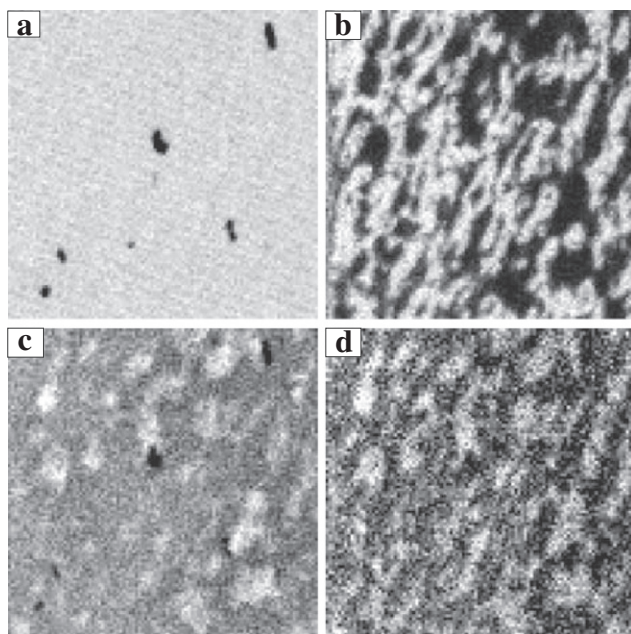

FIGURE 3.20   Scanning transmission X-ray micrographs ($10\mu m^2$) of polybutadiene/ poly(isobutylene-co-4-methylstyrene) (30/70) blend containing 20 phr carbon black, at increasing photon energies: (a) lowest energy—only carbon black structure evident; (b) higher energy— unsaturated polymer also evident; (c) and (d) highest photon energies—polyisobutylene now apparent with reversed contrast. Darker regions in the images depict locations of higher absorbing material and lighter regions are more transparent (Winesett et al., 2003).

A simple method of determining whether the phase morphology is homogeneous is by calorimetry. Observation of two transitions, corresponding to the respective T_g of each component, indicates a phase-separated morphology. However, a single transition does not guarantee thermodynamic miscibility, especially if the component T_gs are close. On the other hand, spectroscopic measurements can reveal two distinct relaxation peaks, even for a thermodynamically miscible blend (Miller et al., 1990; Roland and Ngai, 1991; Alegria et al., 1994; Ngai and Roland, 1995). Referred to as "dynamic heterogeneity," this arises when the components have very different intrinsic mobilities. The motion of each component is determined both by its chemical composition and by its local environment. The latter is averaged out when the phase morphology is homogeneous, which usually results in a single blend T_g. However, if the intrinsic mobilities are very different, two transitions can be observed, as shown in Figure 3.21. The transition, measured either by calorimetry or relaxation spectroscopy, of dynamically heterogeneous, miscible blends is usually quite broad (Roland, 1987).

When the respective component glass transition temperatures are close, the blend T_g is not a useful measure of blend homogeneity. In fact, excess mixing volumes and specific interactions can cause anomalous behavior. The T_g of such a blend can be lower (as seen in polychloroprene/epoxidized polyisoprene blends (McGrath and Roland, 1994)) or higher (as seen in polylepichlorohydrin/polyvinylmethylether blends (Alegria et al., 1995)), than T_g of either neat component. In blends of polymers having nearly equivalent
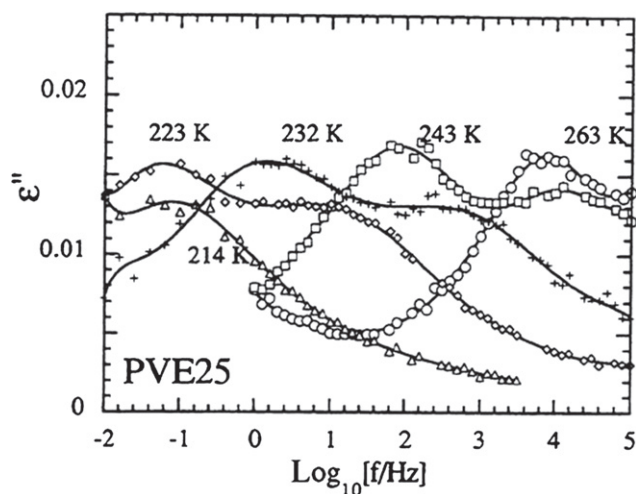

FIGURE 3.21 Isothermal dielectric loss curves for a thermodynamically-miscible blend of 25% 1,2-polybutadiene with natural rubber. Notwithstanding the homogenous morphology, the respective mobilities of the components differ, whereby two peaks are observed in the spectrum. Reprinted from Alegria et al. (1994).
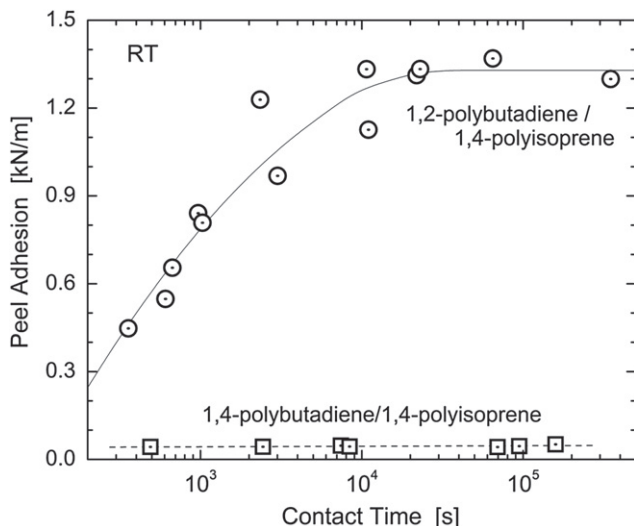
FIGURE 3.22 Resistance to separation of strips of two miscible rubbers (circles) and two immiscible rubbers (squares). Whereas adhesion of the latter remains low, the former is time dependent as the chains interdiffuse. At long times the interface is gone and the peel adhesion becomes constant (Roland, 1987).

T_g, spontaneous interdiffusion of the two materials can serve as an indication of thermodynamic miscibility (Figure 3.22; Roland, 1987).

^{129}Xe NMR has proven useful as a probe for blends (Miller, 1993). Xenon is highly polarizable, so that even van der Waals interactions produce large changes in its NMR chemical shift. When dissolved in a heterogeneous polymer blend, two ^{129}Xe NMR lines are observed, if the domains are large (relative to the diffusion time of the xenon). On the other hand, a single resonance is consistent with miscibility and yields an upper bound on the domain size. The technique is most useful for rubbery materials, so that the spectral lines are sharp. Various groups have used ^{129}Xe NMR to investigate the phase morphology of blends (Wachowicz et al., 2008; Wolak et al., 2003; Miyoshi et al., 2002; da Silva et al., 2000; Walton et al., 1992, 1993; McGrath and Roland, 1994). Figure 3.23 shows the changes in the ^{129}Xe NMR spectrum during redissolution of a blend of 1,4-polyisoprene and 1,4-polybutadiene after heating above the lower critical solution temperature (LCST).

A problem with phase-separated blends is obtaining a uniform dispersion of the compounding ingredients. For example, the distribution of curatives can be skewed by diffusion from one phase into the other. This problem is more significant when the component polymers have substantially different solubility parameters. Various methods have been proposed to assess the crosslink distribution in rubber blends (Tinker, 1995). Since the glass transition behavior is affected by vulcanization, especially for high degrees of crosslinking,
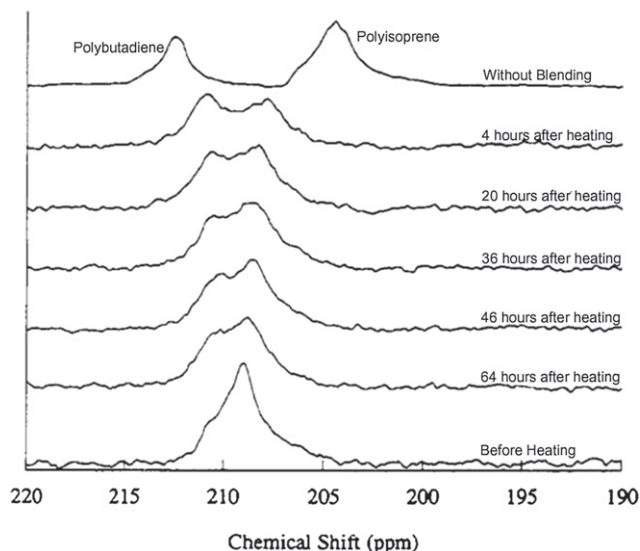
FIGURE 3.23 NMR spectra of ^{129}Xe dissolved in a homogeneous blend (bottom), and at various times after heating above the LCST, whereby phase separation transpires. The uppermost curve was measured on the pure polymers, simultaneously in the NMR tube but physically separated (Walton et al., 1993).

measurement of T_g (Shutilin, 1985; Tinker, 1990) or the local segmental relaxation (Roland, 1994) of the components can yield information about crosslink distributions. However, the method is insensitive for low degrees of crosslinking and requires that the components have significantly different T_gs. If the crosslinking is low enough that a substantial fraction of the polymer remains soluble, analysis of the respective sol and gel fractions can potentially enable the relative crosslinking of the phases to be assessed (Shvydkaya et al., 1980). There have been attempts to use TEM of swollen rubber blends to investigate crosslink distributions (Tinker, 1995). NMR imaging can detect spatially varying crosslink densities. Although the technique has been applied to study oxidation of rubber (Blumler and Blumich, 1997), the spatial resolution is too coarse (>10 µm) for blend studies.

NMR of swollen rubber has been used to determine crosslink distributions in blends (Loadman and Tinker, 1989; Brown et al., 1992; Cook, 1999). Swelling enhances chain mobility, and the isotropic motion of nuclei averages local fields, thereby narrowing the spectral lines. This allows individual resonances to be characterized. Crosslinking constrains motion and makes it more anisotropic, and thereby the incoherent averaging is less complete, broadening line widths (Figure 3.24). Empirical correlations with crosslink density are required for quantitative results. A variation on this technique is the use of ^{129}Xe, taking advantage of the shift dependence on the crosslink density (Parker et al., 2007).
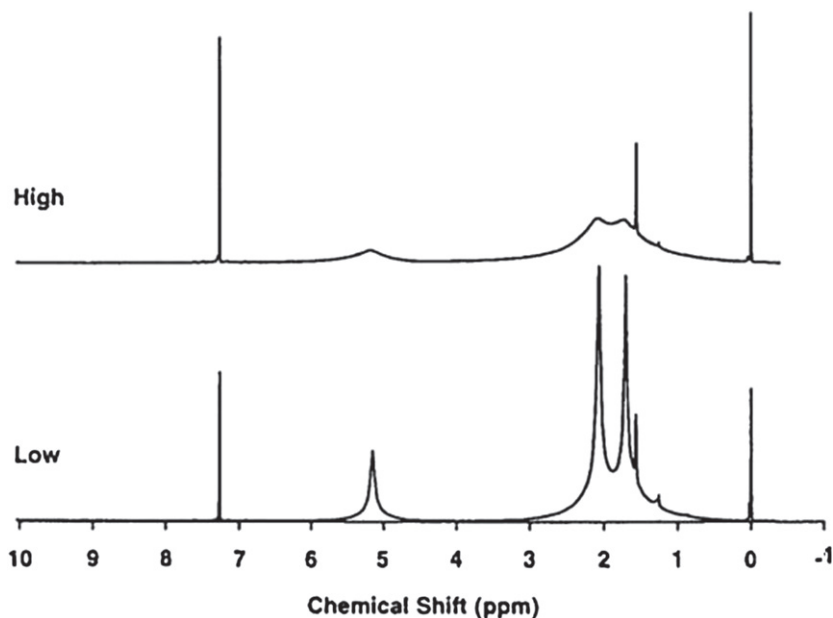
FIGURE 3.24 ^{1}H NMR spectra of swollen NR elastomers. The spectrum in the upper panel is for a sample having a crosslink density 4.5 times larger than that for the lower panel. The resonance at 5.2 ppm, due to the olefinic protons, can be utilized to determine relative crosslink densities (Tinker, 1995).

Crystallization in miscible blends can occur with rejection of the noncrystallizing component, so that its concentration in the amorphous phase increases. Alternatively, if it can be accommodated in the unit cell, it may be entrapped, with consequent alteration in the mean unit cell volume (Tomlin and Roland, 1993). In NR, there is also a shift to formation from α-lamellae to the β-lamellar form (Zemel and Roland, 1992b) (Figure 3.25). These crystal structures have the same unit cell, but the latter has a greater fold-surface free energy. Thus, the noncrystallizing blend component is more readily accommodated into the fold plane at the crystal surface.

3.6.3 Crystallinity

Rubbery behavior—large, reversible extensibility—implies an absence of crystallinity, and this is usually the case for undeformed elastomers. However, small extents of crystallization may be present at ambient temperature in some elastomers, including EPDM with high ethylene content, epichlorohydrin rubber, and polypropylene oxide. The crystallites in these materials can act as reinforcing agents. Many thermoplastic elastomers have crystalline domains that function as reversible crosslinks (Rzymski and Radusch, 2005; Bhowmick and Stephens, 2001).
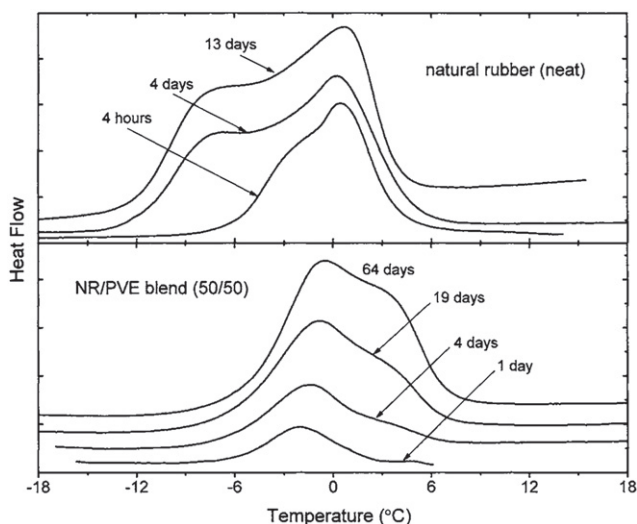
FIGURE 3.25   DSC melting endotherms in NR, pure (upper panel) and blended 50/50 with 1,2-polybutadiene (lower panel), after crystallization at −25 °C for the indicated time periods. The neat rubber initially crystallizes into the more stable α-lamellae, with substantial β-lamellae only forming at higher extents of crystallization. Miscible blending causes preferential crystallization of the lower melting β-lamellae (Zemel and Roland, 1992b).

If there is sufficient regularity of their backbone structure, amorphous rubbers crystallize at lower temperatures; this mainly affects storage behavior. Unoriented NR crystallizes through lamellar growth into radial spherulites, having two morphologically differing forms, the more stable α-lamella and the slower forming β-lamella (Andrews et al., 1971). Both lamellar types have the same crystal unit cell, but differ with respect to growth rates, lamellar thicknesses, and morphologies. As mentioned, the β-lamella have a higher fold-surface free energy. In order to accommodate the presence of *trans* units, synthetic *cis*-1,4-polyisoprene tends to crystallize more in the β-form, since the fold surface better tolerates noncrystallizing units (Edwards, 1975). A similar alteration in the crystal morphology of 1,4-polyisoprene is caused by miscible blending (see Figure 3.23) (Zemel and Roland, 1992b).

Although elastomers are usually amorphous, strain-induced crystallization occurs in rubbers such as *cis*-1,4-polybutadiene, butyl rubber, and NR, the most important commercial elastomer. Crystallization under stress, discovered 200 years ago (Gough, 1805), increases the modulus and most failure properties of rubber, and is essential to performance in many applications (Magill, 1995; Gent and Zhang, 2002; Hamed and Rattanasom, 2002; Santangelo and Roland, 2001). For NR, the propensity for strain-crystallization correlates directly with the failure properties (Choi and Roland, 1996). Crystallization of natural rubber under strain transpires through row nucleation of lamellae, whose growth proceeds perpendicular to the strain direction (Edwards,

1975; Andrews et al., 1971). The latter, secondary crystallization, can be quite slow (Mitchell and Meier, 1968), and its rate is unaffected by strain (Andrews et al., 1971). However, the row nucleation rate is greatly enhanced by orientation, effecting rapid initial crystallization (Krigbaum and Roe, 1964; Ziabicki and Jarecki, 1978; Elyashevich, 1982; Roland and Sonnenschein, 1991). The time for strain-induced crystallization of NR is less than 60 ms at RT (Mitchell and Meier, 1968), so that synchrotron X-ray sources (Toki et al., 2003, 2011) are required for on-the-fly measurements.

A prerequisite for high levels of strain-crystallization is steric purity of the polymer backbone, and this accounts for the better performance of natural in comparison to synthetic *cis*-1,4-polyisoprene (Brock and Hackathorn, 1972; Cooper and Smith, 1963). Reinforcing filler influences the crystallization behavior (Trabelsi et al., 2003a; Mark, 2003; Sharaf et al., 1995; Hamed and Park, 1999), as do the other compounding ingredients. The denatured proteins and other hydrocarbon-insoluble contaminants in NR primarily affect the rate of crystallization. For example, it has been shown that acetone extraction (Gent, 1955) and deproteinization of natural rubber (Burfield, 1984) both reduce the isotropic crystallization rate, presumably by reducing nucleation sites. In contrast, the degree of crystallinity attained in the absence of orientation is governed by the backbone microstructure, specifically the length of *cis*-1,4 sequences, not by the nonrubber constituents (Burfield and Tanaka, 1987).

Since the presence of impurities primarily affects crystal nucleation rather than growth (Gent, 1954, 1955), the degree of crystallinity and its dependence on
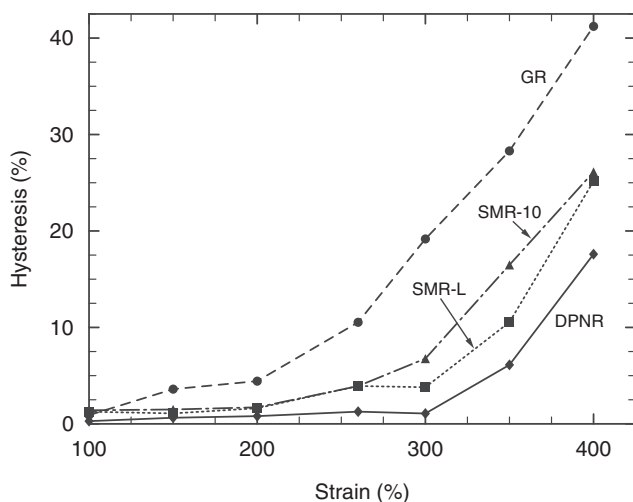

FIGURE 3.26   The mechanical energy dissipated relative to the total input strain energy for four grades of NR, stretched at RT to various extent. Strain crystallization at ca. 250% or higher results in more marked hysteresis (Choi and Roland, 1997).
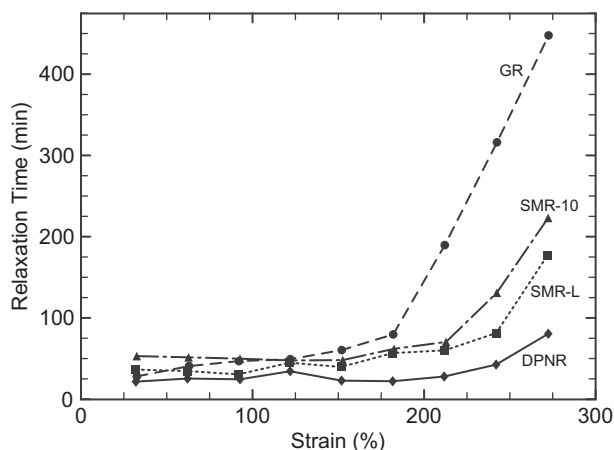
FIGURE 3.27   The time over which stress decay was observed for four NR elastomers. Initially viscoelasticity governs the relaxation time; at higher strains crystallization commences (Choi and Roland, 1997).

strain are of less interest in accounting for the failure properties of rubber. However, the minimum strain required for crystallization determines the stress concentration necessary to induce crystallization in the vicinity of a crack, as well as its spatial extent. Thus, this minimum strain plays a governing role in mechanical performance. Among the various grades of NR, the greater the purity, the higher the strain required to induce crystallization (Choi and Roland, 1997).

Methods to study crystallization of deformed elastomers include X-ray diffraction (Toki et al., 2003, 2011; Mitchell, 1984; Oono et al., 1973; Trabelsi et al., 2003b), optical birefringence (Treloar, 1947; Taylor and Darin, 1955), infrared or Raman spectroscopy, electron microscopy (Shimizu et al., 1998), dilatometry (Gent and Zhang, 2001, 2002), NMR (Kameda and Asakura, 2003), and mechanical measurements (Choi and Roland, 1997; Gent, 1954). Strain-induced crystallization is manifested in the latter by both greater hysteresis (Figure 3.26) and a longer time for stress decay (Figure 3.27). However, the shape of the stress-strain curve during extension does not obviously reveal the onset of crystallization (Toki et al., 2003, 2011; Choi and Roland, 1997).

3.6.4 Defects

It is well known that elastomers, like virtually all solid materials, have preexisting, "naturally occurring" flaws (Roland and Smith, 1985). By intensifying local stresses, such flaws exert an influence on the failure properties of elastomers. More recently, interest in these flaws has increased, due to concerns about their potential for reducing the barrier performance of rubber films. This performance is crucial in the use of latex rubber products, such as surgical

gloves and condoms, to block transmission of the submicron-sized particles responsible for AIDS, hepatitis, and other viral diseases (Roland, 1993).

The passage of viral-sized particles through ostensibly intact NR latex films has been directly observed in the laboratory (Carey et al., 1992; Kiernan, 1996), and indirectly observed in the field (The New York Times, 1994). Evidence for such flaws in NR comes from microscopic observations (Arnold et al., 1988), as well as water absorption measurements, wherein the initial rapid uptake suggests the existence of capillary channels (Gazeley et al., 1988).

Since failure properties are affected by the intrinsic defects in rubber, they offer a means to characterize these flaws. The strength of rubber is influenced by the presence of defects having an apparent size in the range between 5 and 70 µm (Bueche, 1959; Braden and Gent, 1960; Gent, 1978; Roland and Sobieski, 1989). Thus, a means to estimate the size of the largest inherent flaw is by measuring the strength of samples after the introduction of cuts of varying size. The data are extrapolated to the strength of the uncut material, to yield the inherent crack size. If the rubber strain-crystallizes, the precuts must be small, so that such crystallization of the bulk material transpires prior to failure (Thomas and Whittle, 1970). For a linearly elastic material, the strength will vary as the square-root of the flaw size (Gent, 1978), while more generally, the strain energy to break is proportional to the flaw size (Bell et al., 1982). In Table 3.4 the flaw size deduced from the strain energy to break is listed for various grades of NR (Choi and Roland, 1996).

Since fatigue failure of rubber is envisioned as growth of intrinsic flaws, measurement of fatigue lifetimes (e.g., deformation cycles to failure) can provide a measure of the intrinsic flaw size (Gent et al., 1964; Lake and Lindley, 1965; Lake, 1983). Table 3.4 includes the flaw sizes determined from the fatigue life of these sample NR compounds (Choi and Roland, 1996).

The values determined for the inherent flaws only represent effective sizes, corresponding to a given degree of stress concentration (Greensmith, 1964). This stress concentration also depends on the shape of a crack (e.g., bluntness), as well as the dissipative capacity of the material itself (Hamed et al., 1996). Although compounding variables such as crosslink density strongly affect the

TABLE 3.4 Intrinsic Flaw Size of Natural Rubbers (Choi and Roland, 1996)

NR Grade	Intrinsic Flaw Size (µm)	
	Strain Energy	Fatigue Life
Guayule rubber	29	26
SMR-10	29	31
SMR-L	26	17
Deproteinized NR	16	10

failure properties of rubber, their influence on the intrinsic defect size is more modest (Lake and Lindley, 1965; Lake, 1983; Hamed, 1983). The measured flaw size is unaffected by temperature (Braden and Gent, 1960), although it can vary with carbon black type (Dizon et al., 1973). The degree of dispersion of compounding ingredients can influence the strength of rubber, apparently by a flaw-initiation mechanism (May, 1964).

ACKNOWLEDGMENTS

REFERENCES

Abdel-Goad, M., Pyckhout-Hintzen, W., Kahle, S., Allgaier, J., Richter, D., Fetters, L.J., 2004. Macromolecules 37, 8135.
Akcasu, A.Z., Summerfield, G.C., Jahsan, S.N., Han, C.C., Kim, C.Y., Yu, H., 1980. J. Polym. Sci. Polym. Phys. 18, 863.
Alegria, A., Colmenero, J., Ngai, K.L., Roland, C.M., 1994. Macromolecules 27, 4486.
Alegria, A., Elizetxea, C., Cendoya, I., Colmenero, J., 1995. Macromolecules 28, 8819.
Andrews, E.H., Owen, P.G., Singh, A., 1971. Proc. Royal Soc. London A 324, 79.
Annis, B.K., Kim, M.H., Alamo, R., Pyda, M., 2001. J. Polym. Sci. Polym. Phys. 39, 2852.
Arbe, A., Colmenero, J., Farago, B., Monkenbusch, M., Buchenau, U., Richter, D., 2003. Chem. Phys. 292, 295.
Arnold, S.G., Whitman, J.E., Fox, C.H., Cottler-Fox, M.H., 1988. Nature 335, 19.
Avgeropoulos, G.N., Weissert, F.C., Biddison, P.H., Bohm, G.G.A., 1976. Rubber Chem. Technol. 49, 93.
Baldwin, F.P., Ver Strate, G., 1972. Rubber Chem. Technol. 44, 709.
Balke, S.T., Mourey, T.H., 2001. J. Appl. Polym. Sci. 81, 370.
Barth, H., Mays, J., 1991. Modern Methods of Polymer Characterization. Wiley, New York.
Bell, C.L.M., Stinson, D., Thomas, A.G., 1982. Rubber Chem. Technol. 55, 66.
Berger, L., Kausch, H.H., Plummer, C.J.G., 2003. Polymer 44, 5877.
Berne, B.J., Pecora, R., 1976. Dynamic Light Scattering. Wiley, New York (Chapter 8).
Betrand, P., Weng, L.T., 1999. Rubber Chem. Technol. 72, 384.
Betrand, P., Weng, L.T., Lauer, W., Zimmer, R., 2002. Rubber Chem. Technol. 75, 627.
Bhowmick, A.K., Stephens, H.L. (Eds.), 2001. Handbook of Elastomers, 2nd ed. Marcel Dekker, New York.
Blitz, J.P., McFaddin, D.C., 1994. J. Appl. Polym. Sci. 51, 13.
Blumler, P., Blumich, B., 1997. Rubber Chem. Technol. 70, 468.
Bogoslovov, R.B., Hogan, T.E., Roland, C.M., 2010. Macromolecules 43, 2904.
Bohm, G.G.A., Tveekrem, J.O., 1982. Rubber Chem. Technol. 55, 575.
Bonnar, R.U., Dimbat, M., Stross, F.H., 1958. Number-Average Molecular Weights—Fundamentals and Determination. Interscience, New York, NY.
Bonse, U., Hart, M., 1965. Appl. Phys. Lett. 7, 238.
Booth, C., Price, C. (Eds.), 1989. Comprehensive Polymer Science, vol. 1. Polymer Characterization, Pergammon, NY.
Boothroyd, A., Fetters, L.J., 1991. Macromolecules 24, 5215.
Botti, A., Pyckhout-Hintzen, W., Richter, D., Urban, V., Straube, E., Kohlbrecher, J., 2003. Polymer 44, 7505.
Boue, G., Bastide, J., Buzier, M., Lapp, A., Herz, J., Vilgis, T.A., 1991. Coll. Polym. Sci. 269, 195.
Bower, D.I., 1981. J. Polym. Sci. Polym. Phys. 19, 93.
Bower, D.I., Lewis, E.L.V., Ward, I.M., 1995. Polymer 36, 3473.
Braden, M., Gent, A.N., 1960. J. Appl. Poly. Sci. 3, 100.

Braun, D., 1996. Simple Methods for Identification of Plastics, 3rd ed. Hanser, NY.

Braun, D., Rettig, R., Rogler, W., 1993. Angew. Makromol. Chem. 211, 165

Briggs, D., 1989. Brit. Polym. J. 21, 3.

Brock, M.J., Hackathorn, M.J., 1972. Rubber Chem. Technol. 45, 1301.

Brosseau, C., Molinie, P., Boulic, F., Carmona, F., 2001. J. Appl. Phys. 89, 8297.

Brown, J., Verdier, P., 1972. J. Res. Natl. Bur. Stand. A76, 161.

Brown, P.S., Loadman, M.J.R., Tinker, A.J., 1992. Rubber Chem. Technol. 65, 744.

Bruell, R., Raquel, M., Rode, K., 2010. Macro. Chem. Phys. 211, 2233.

Brun, Y., 1998. J. Liq. Chromatography & Related Technol. 21, 1979.

Bueche, F., 1959. Rubber Chem. Technol. 32, 1269.

Bur, A.J., Roth, S.C., Thomas, C.L., 2000. Rev. Sci. Instr. 71, 1516.

Burfield, D.R., 1984. Polymer 25, 1823.

Burfield, D.R., Tanaka, Y., 1987. Polymer 28, 907.

Campbell, D., White, J., 1989. Polymer Characterization. Chapman and Hall, NY.

Capancioni, S., Schwach-Abdellaoui, K., Kloeti, W., Herrmann, W., Brosig, H., Borchert, H.H., Heller, J., Gurny, R., 2003. Macromolecules 36, 6135.

Carella, J.M., Gotro, J.T., Graessley, W.W., 1986. Macromolecules 19, 659.

Carey, R.F., et al., 1992. Sexually Transmitted Diseases 19, 230.

Casassa, E., 1972. Polym. J. 3, 517.

Castignolles, P., Gaborieau, M., 2010. J. Separation Sci. 33, 3564.

Cebe, P., 2005. J. Polym. Sci. Polym. Phys. Ed. 43, 629.

Chen, X., Xi, J., Guo, B.H., 2006. J. Appl. Polym. Sci. 102, 3201.

Cheng, H., 1991. In: Barth, H., Mays, J. (Eds.), Modern Methods of Polymer Characterization, Chemical Analysis, vol. 113. Wiley, N.Y., p. 409.

Cheng, M.H.Y., Nauman, E.B., 2004. J. Polym. Sci. Polym. Phys. 42, 603.

Cho, D., Park, S., Kwon, K., Chang, T., Roovers, J., 2001. Macromolecules 34, 7570.

Choi, I.S., Roland, C.M., 1996. Rubber Chem. Technol. 69, 591.

Choi, I.S., Roland, C.M., 1997. Rubber Chem. Technol. 70, 202.

Chou, C.Y., Hsieh, Y.H., Chang, G.G., 2011. Methods 54, 76.

Clough, R.S., Koenig, J.L., 1989. Rubber Chem. Technol. 62, 908.

Colby, R.H., Fetters, L.J., Graessley, W.W., 1987. Macromolecules 20, 2237.

Collins, E., Bares, J., Billmeyer, F., 1973. Experiments in Polymer Science. Wiley, NY.

Cook, S., 1999. Kaut. Gummi Kunst. 52, 350.

Cooper, A. (Ed.), 1989. Determination of Molecular Weight, Chemical Analysis Series, vol. 103. Wiley, New York.

Cooper, W., Smith, R.K., 1963. J. Polym. Sci. A 1, 159.

Creel, H., 1993. Trends Polym. Sci. 1, 336.

da Silva, N.M., Tavares, M.I.B., Stejskal, E.O., 2000. Macromolecules 33, 115.

Dawkins, J.V. (Ed.), 1986. Developments in Polymer Characterization, vol. 1–5. Elsevier, NY.

Dekmezian, A., Morioka, T., Campo, C., 1990. J. Pol. Sci. Phys. 28, 1908.

Dekmezian, A., Morioka, T., Campo, C., 1990. J. Polym. Sci. Polym. Phys. 28, 1908.

Deloche, B., Samulski, E.T., 1981. Macromolecules 14, 575.

Devries, K.L., 1971. J. Polym. Sci. C Polym. Symp. 32, 325.

Dieing, T., Hollricher, O., Toporski, J. (Eds.), 2011. Confocal Raman Microscopy, Springer.

Dizon, E.S., Hicks, A.E., Chirico, V.E., 1973. Rubber Chem. Technol. 46, 231.

Doi, M., 1993. In: Thomas, E.L. (Ed.), Structure and Properties of Polymers. Wiley-VCH (Weinheim).

Doi, M., Watanabe, H., 1991. Macromolecules 24, 740.

Dumas, P.J., 2003. de Phys. IV 104, 359.

Dupres, S., Long, D.R., Albouy, P.A., Sotta, P., 2009. Paul. Macromolecules 42, 2634.

Edwards, B.C., 1975. J. Polym. Sci., Polym. Phys. 13, 1387.

Ekanayake, P., Menge, H., Schneider, H., Ries, M.E., Brereton, M.G., Klein, P.G., 2000. Macromolecules 33, 1807.

Elyashevich, G.K., 1982. Adv. Poly. Sci. 43, 205.

Everall, N.J., Bibby, A., 1997. Appl. Spect. 51, 1083.

Feast, W.J., Keeney, A.J., Kenwright, A.M., Parker, D., 1997. Chem. Comm. 18, 1749.

Feng, Y., Hay, J.N., 1998. Polymer 39, 6723.

Flory, P.J., 1969. Statistical Mechanics of Chain Molecules. Oxford Univ. Press, NY.

Fox, T.G., Flory, P.J., 1954. J. Polym. Sci. 14, 315.

Froud, C.A., Hayward, I.P., Laven, J., 2003. Appl. Spect. 57, 1468.

Fuhrmann, I., Karger-Kocsis, J., 2003. J. Appl. Polym. Sci. 89, 1622.

Fulton, S.W., 2006. Rubber Chem. Technol. 79, 790.

Gaborieau, M., Gilbert, R.G., Gray-Weale, A., Hernandez, J.M., Castignolles, P., 2007. Macro. Theor. Simul. 16, 13.

Garcia, R.A., Coto, B., Exposito, M.T., Suarez, I., Fernandez-Fernandez, A., Caveda, S., 2011. Macromol. Res. 19, 778.

Gazeley, K.F., Gorton, A.D.T., Pendle, T.D., 1988. In: Roberts, A.D. (Ed.), Natural Rubber Science and Technology. Oxford Univ. Press Oxford (Chapter 3).

Gent, A.N., 1954. Inst. Rubb. Ind. 30, 139.

Gent, A.N., 1954. Trans. Faraday Soc. 50, 521.

Gent, A.N., 1955. J. Polym. Sci. 18, 321.

Gent, A.N., 1978. In: Eirich, F.R. (Ed.), Science and Technology of Rubber. Academic Press, New York (Chapter 10).

Gent, A.N., Zhang, L.Q., 2001. J. Polym. Sci. Polym. 39, 811.

Gent, A.N., Zhang, L.Q., 2002. Rubber Chem. Technol. 75, 923.

Gent, A.N., Lindley, P.B., Thomas, A.G., 1964. J. Appl. Poly. Sci. 8, 455.

Ghanbari-Siahkali, A., Almdal, K., Kingshott, P., 2003. Appl. Spect. 57, 1482.

Ghebremeskel, G.N., Sekinger, J.K., Hoffpauir, J.L., Hendrix, C., 1996. Rubber Chem. Technol. 69, 874.

Glockner, G., 1989. In: Booth, C., Price, C. (Eds.), Comprehensive Polymer Science, vol. 1. Polymer Characterization. Pergammon, New York, 1989. p. 313.

Goga, N.O., Demco, D.E., Kolz, J., Ferencz, R., Haber, A., Casanova, F., Bluemich, B., 2008. J. Mag. Res. 192, 1.

Gough, J., 1805. Proc. Lit. and Phil. Soc. Manchester, 2nd Ser., 1, 288.

Graessley, W., Ver Strate, G., 1980. Rubber Chem. Technol. 53, 842.

Greensmith, H.W., 1964. J. Appl. Polym. Sci. 8, 1113.

Grest, G.S., Fetters, L.J., Huang, J.S., Richter, D., 1996. In: Prigogine, I., Rice, S.A. (Eds.), Advances in Chemical Physics XCIV. Wiley, NY 1996.

Gronski, W., Forster, F., Pyckhout-Hintzen, W., Springer, T., 1990. Makromolekulare Chem. Macromol. Symp. 40, 121.

Grubisic, Z., Rempp, P., Benoit, H., 1967. J. Polym. Sci. 21, 753.

Grubsic-Gallot, Z., Lingelser, J.P., Gallot, Y., 1990. Polym. Bull. 23, 389.

Grum, F., 1972. In: Weissberger, A., Rossiter, B. (Eds.). Visible and Ultraviolet Spectrophotometry. Physical Methods of Chemistry, Part III B. vol. 1. Wiley lnterscience, New York, p. 207.

Hamed, G.R., 1983. Rubber Chem. Technol. 56, 244.

Hamed, G.R., Park, B.H., 1999. Rubber Chem. Technol.72, 946.

Hamed, G.R., Rattanasom, N., 2002. Rubber Chem. Technol. 75, 935.

Hamed, G.R., Kim, H.J., Gent, A.N., 1996. Rubber Chem. Technol. 69, 807.

Hammond, T., Lehrie, R., 1989. Brit. Polym. J. 21, 23.

Hammouda, B., 2010. J. Macromol. Sci. C 50, 14.

Hauck, D., Fink, G., Chwatinski, C., Blumler, P., Blumich, B., Unseld, K., 1997. Kauch. Gummi Kunstat. 50, 392.

Hennecke, M., Kurz, K., Fuhrmann, J., 1992. Macromolecules 25, 6190.

Higgins, J.S., Benoit, H.C., 1997. Polymers and Neutron Scattering. Clarendon Press, Oxford.

Hinojosa, O., Arthur, J.C., Nakamura, Y., 1972. J Polym. Sci. C Polym. Symp. 37, 27.

Hohne, G., Merzlyakov, M., Schick, C., 2002. Thermochim. Acta 391, 51.

Hommel, H., Touhami, A., Legrand, A.P., 1993. Makromol. Chem. Macro. Chem. Phys. 194, 879.

Horsky, J., Bohdanecky, M., 1990. Eur. Pol. J. 26, 1190.

Hoven, V.P., Rattanakaran, K., Tanaka, Y., 2003. Rubber Chem. Technol. 76, 1128.

Hsu, S.L., 2004. Handbook of Vibrational Spectroscopy: A Companion for Polymer Scientists. Wiley, NY

Hu, J.C., 1981. Anal. Chem. 53, 942.

Hutchinson, J.M., 2003. J. Therm. Anal. Calorimetry 72, 619.

Ishida, H., 1987. Rubber Chem. Technol. 60, 497.

Janca, J., Ananieva, I.A., Menshikova, A.Y., Evseeva, T.G., 2004. J. Chromatography B800, 33.

Jiang, S., Bae, S.C., Granick, S., 2008. Langmuir 24, 1489.

Kameda, T., Asakura, T., 2003. Polymer 44, 7539.

Kannan, R.M., Kornfield, J.A., 1994. J. Rheol. 38, 1127.

Karabudak, E., Wohlleben, W., Colfen, H., 2010. Eur. Biophys. J. 39, 397.

Kassalainen, G.E., Williams, S.K.R., 2003. Anal. Chem. 75, 1887.

Kawahara, S., Inomata, Y., Kakubo, T., Tanaka, Y., Hatada, K., Ute, K., Miyatake, N., 1998. Rubber Chem. Technol. 71, 277.

Keilman, F., 2002. Vibr. Spect. 29, 109.

Keilmann, F., 2003. J. Biol. Phys. 29, 195.

Kempfert, K.D., Coel, B., Troost, P., Lavery, D.S., 2001. Amer. Lab. 33, 22.

Kiernan, V., 1996. New Scientist, March 23, p. 7.

Kim, W.S., Eum, C.H., Molnar, A., Yu, J.S., Lee, S., 2006. Analyst 131, 429.

Kinsey, R., 1990. Rubber Chem. Technol. 63, 407.

Koenig, J.L., 1999. Spectroscopy of Polymers, 2nd ed. Elsevier, NY.

Koenig, J.L., 2000. Rubber Chem. Technol. 73, 385.

Kona, B., Weidner, S.M., Friedrich, J.F., 2005. Int. J. Polym. Anal. Char. 10, 85.

Kotani, M., Dohi, H., Kimura, H., Muraoka, K., Kaji, H., 2007. Macromolecules 40, 9451.

Kraus, G., Gruver, J.T., 1965. J. Polym. Sci. A 3, 105.

Kremer, F., Schonhals, A. (Eds.), 2003. Broadband Dielectric Spectroscopy. Springer, Berlin.

Krigbaum, W.R., Roe, R.J., 1964. J. Polym. Sci. A2, 4391.

Krishnan, R., Nagarajan, K., 2010. J. Therm. Anal. Cal. 102, 1135.

Kuo, C.Y., Provder, T., 1987. ACS Symp. Series 352, 2.

Kuo, C.Y., Provder, T., Koehler, M.E., 1990. J. Liq. Chromatography 13, 3177.

Kuo, C.Y., Provder, T., Koehler, M.E., 1993. ACS Symp. Series 521, 231.

Kurata, M., Tsunashima, Y., 1999. In: Brandrup, J., Immergut, E.H., Grulke, E.A. (Eds.), Polymer Handbook, 4th ed. Wiley, New York (Chapter 7).

Lake, G.J., 1983. Prog. Rubber Technol. 45, 89.

Lake, G.J., Lindley, P.B., 1965. J. Appl. Poly. Sci. 9, 1233.

Lattimer, R., 1990. Rubber Chem. Technol. 63, 298.

Laue, T.M., 1990. In: Kroschwitz, J.I. (Ed.), Concise Encyclopedia of Polymer Science and Engineering. Wiley, New York, 1990, p. 1225.

Lee, S.H., Molnar, A., 1995. Macromolecules 28, 6354.

Lee, D., Williams, S.K.R., 2010. J. Chromat. 1217, 1667.

Lee, S., Eum, C.H., Plepys, A.R., 2000. Bull. Korean Chem. Soc. 21, 69.

Leeson, A.M., Alexander, M.R., Short, R.D., Briggs, D., Hearn, M.J., 1997. Surf. Interfac. Anal. 25, 261.

Lewandowski, L., Sibbald, M.S., Johnson, E., Mallamaci, M.P., 2000. Rubber Chem. Technol. 73, 731.

Lindner, H., Glatter, O., 2000. Macromol. Symp. 162, 81.

Litvinov, V.M., Orza, R.A., Klueppel, M., van Duin, M., Magusin, P.C.M.M., 2011. Macromolecules 44, 4887.

Loadman, M.J.R., Tinker, A.J., 1989. Rubber Chem. Technol. 62, 234.

Lohse, D.J., 1994. Rubber Chem. Technol. 67, 367.

Madan, B., Naskar, N.K., Perera, K., Moreland, C., Hodge, T., Wallace, K., Beckham, H.W., Smith, D.W., 2012. Rubber Chem. Technol. 85, 68.

Maeda, Y., Yamamoto, H., Ikeda, I., 2003. Macromolecules 36, 5055.

Magill, J.H., 1995. Rubber Chem. Technol. 68, 507.

Majeste, J.C., Carrot, C., Stanescu, P., 2003. Rheo. Acta 42, 432.

Mark, J.E., 2003. Prog. Polym. Sci. 28, 1205.

Mathew, T., Datta, R.N., Dierkes, W.K., Noordermeer, J.W.A., van Ooij, W.J., 2008. Rubber Chem. Technol. 81, 209.

Mathot, V., Pyda, M., Pijpers, T., Poel, G.V., van de Kerkhof, E., van Herwaarden, S., van Herwaarden, F., Leenaers, A., 2011. Thermochim. Acta 522, 36.

May, W., 1964. Trans. Inst. Rubber Ind. 40, T109.

McCarley, K.D., Bunge, A.L., 2003. Int. J. Pharm. 250, 169.

McGrath, K.J., Roland, C.M., 1994. Rubber Chem. Technol. 67, 629.

Medrano, R., Laguna, M.T.R., Saiz, E., Tarazona, M.P., 2003. Phys. Chem. Chem. Phys. 5, 151.

Messaud, F.A., Sanderson, R.D., Runyon, J.R., Ray, J., Otte, T., Pasch, H., Williams, S.K.R., 2009. Prog. Polym. Sci. 34, 351.

Messerschmidt, R., Harthcock, M. (Eds.), 1988. Infrared Microspectroscopy, Practical Spectroscopy Series, vol. 6. Marcel Dekker, NY.

Mileva, D., Androsch, R., Zhuravlev, E., Schick, C., 2009. Macromolecules 42, 7275.

Miller, J.B., 1993. Rubber Chem. Technol. 66, 455.

Miller, G.H., Tobias, R.H., 1978. Rubber Chem. Technol. 51, 977.

Miller, J.B., McGrath, K.J., Roland, C.M., Trask, C.A., Garroway, A.N., 1990. Macromolecules 23, 4543.

Minari, R.J., Rodriguez, V.I., Estenoz, D.A., Vega, J.R., Meira, G.R., Gugliotta, L.M., 2010. J. Appl. Polym. Sci. 116, 590.

Mirabella, F.M., 1993. Polymer 34, 1729.

Mitchell, G.R., 1984. Polymer 25, 1562.

Mitchell, J. (Ed.), 1992. Applied Polymer Analysis and Characterization, vol. 2. Hanser, NY.

Mitchell, J.C., Meier, D.J., 1968. J. Polym. Sci. Polym. Phys. 6, 1689.

Miyoshi, T., Takegoshi, K., Terao, T., 2002. Macromolecules 35, 141.

Mori, M., Koenig, J.L., 1998. J. Appl. Polym. Sci. 70, 1391.

Mori, S., Mouri, M., 1989. Anal. Chem. 61, 2171.

Myers, C.W., Cooper, S.L., 1994. Appl. Spect. 48, 72.

Nagy, D.J., 2003. Amer. Lab. 35, 38.

Ngai, K.L., Paluch, M., 2004. J. Chem. Phys. 120, 857.

Ngai, K.L., Plazek, D.J., 1995. Rubber Chem. Technol. 68, 376.

Ngai, K.L., Roland, C.M., 1995. Macromolecules 28, 44033.

Ngai, K.L., Roland, C.M., 1997. J. Polym. Sci. Polym. Phys. 35, 2503.

Nguyen, M., Beckett, R., Pille, L., Solomon, D.H., 1998. Macromolecules 31, 7003.

Nielsen, M.W.F., 1999. Mass. Spectrom. Rev. 18, 309.

Okabe, M., Mitsui, K., Oranaka, H., Jahahashi, M., Masuda, H., 1992. Polymer J. 24, 653.

Oono, R., Miyasaka, K., Ishikawa, K., 1973. J. Polym. Sci. 11, 1477.

Pace, M.D., Roland, C.M., 1991. Polymer 32, 1027.

Palanker, D.V., Simanovskii, D.M., Huie, P., Smith, T.I., 2000. J. Appl. Phys. 88, 6808.

Parker, W.O., Ferrando, A., Ferri, D., Canepari, V., 2007. Macromolecules 40, 5787.

Park, M.S., Wong, Y.S., Park, J.O., Venkatraman, S.S., Srinivasarao, M., 2011. Macromolecules 44, 2120.

Partridge, R., Symons, M.C.R., Wyatt, J.L., 1993. J. Chem. Soc. Faraday Trans. 89, 1285.

Paul, D.R., Barlow, J.W., 1980. J. Macromol. Sci. Rev. Macromol. Chem. C18, 108.

Peckj, M.C.P., Samus, M.A., Killgoar, R.C., Carter, R.O., 1991. Rubber Chem. Technol. 64, 610.

Peng, X., Huang, Y., Xia, T., Kong, M., Li, G., 2011. Eur. Polym. J. 47, 1956.

Pielichowski, K., Flejtuch, K., 2002. Polimery 47, 784.

Plazek, D.J., Chay, I.-C., Ngai, K.L., Roland, C.M., 1995. Macromolecules 28, 6432.

Ponomarenko, S.A., Rasulova, N.N., Luponosov, Y.N., Surin, N.M., Buzin, M.I., Leshchiner, I., Peregudova, S.M., Muzafarov, A.M., 2012. Macromolecules 45, 2014.

Provder, T., Urban, M.W., Barth, H.G. (Eds.), 1995. Chromatographic Characterization of Polymers: Hyphenated and Multidimensional Techniques, Adv. Chem. Series 247, Amer. Chem. Soc. Washington, DC.

Puskas, J.E., Hutchinson, R., 1993. Rubber Chem. Technol. 66, 742.

Puskas, J.E., Burchard, W., Heidenreich, A.J., Dos Santos, L., 2012. J. Polym. Sci. Polym. Chem. Ed. 50, 70.

Qu, X.W., Shang, S.R., Liu, G.D., Zhang, S.W., Zhang, Y., Zhang, L.C., 2004. J. Appl. Polym. Sci. 91, 1685.

Rabolt, J.F., Chase, D.B. (Eds.), 2000. Fourier Transform Raman Spectroscopy: From Concept to Experiment. Academic Press, NY.

Ramachandran, R., Beaucage, G., Kulkarni, A.S., McFaddin, D., Merrick-Mack, J., Galiatsator, V., 2008. Macromolecules 41, 9802.

Ramachandran, R., Beaucage, G., McFaddin, D., Merrick-Mack, J., Galiatsatos, V., Mirabella, F., 2011. Polymer 52, 2661.

Raubner, V.M., Jordan, R., Nuyken, O., Lippert, T., Hauer, M., Schnyder, B., Wokaun, A., 2002. Appl. Surf. Sci. 197, 786.

Richter, D., 2003. J. Appl. Cryst.36, 389.

Robertson, C.G., Roland, C.M., Paulo, C., Puskas, J.E., 2001. J. Rheol. 45, 759.

Rodrigues, F.H.A., Santos, E.F., Feitosa, J.P.A., Ricardo, N.M.P.S., de Paula, R.C.M., 2001. Rubber Chem. Technol.74, 57.

Roland, C.M., 1987. Macromolecules 20, 2557.

Roland, C.M., 1993. Rubber World 208, 15.

Roland, C.M., 1994. Macromolecules 27, 4242.

Roland, C.M., 2011. Viscoelastic Behavior of Rubbery Materials. Oxford Univ. Press.

Roland, C.M., Bohm, G.G.A., 1984. J. Polym. Sci. Pt. B-Polym. Phys. 22, 79.

Roland, C.M., Casalini, R., 2003. J. Chem. Phys. 119, 1838.

Roland, C.M., Ngai, K.L., 1991. Macromolecules 24, 2261.

Roland, C.M., Santangelo, P.G., 2002. J. Non-Cryst. Solids 307, 835–841.

Roland, C.M., Smith, C.R., 1985. Rubber Chem. Technol.58, 806.

Roland, C.M., Sobieski, J.W., 1989. Rubber Chem. Technol. 62, 683.

Roland, C.M., Sonnenschein, M.F., 1991. Polym. Eng. Sci. 31, 1434.

Roland, C.M., Ngai, K.L., Santangelo, P.G., Qiu, X.H., Ediger, M.D., Plazek, D.J., 2001. Macromolecules 34, 6159.

Rooney, J.G., Ver Strate, G., 1981. In: Cazes, J. (Ed.), Liquid Chromatography of Polymers and Related Materials III, Marcel Dekker.

Ruch, D., Muller, J.F., Migeon, H.N., Boes, C., Zimmer, R., 2003. J. Mass. Spect. 38, 50.

Ruckebusch, C., Vilmin, F., Coste, N., Huvenne, J.P., 2008. Appl. Spect. 62, 791.

Runt, J.P., Fitzgerald, J.J. (Eds.), 1997. Dielectric Spectroscopy of Polymeric Materials. American Chemical Society, Washington, DC.

Rzymski, W.M., Radusch, H.J., 2005. Polimery 50, 249.

Samperi, F, Battiato, S., Puglisi, C., Scamporrino, A., Ambrogi, V., Ascione, L., Carfagna, C., 2011. J. Polym. Sci. Polym. Chem. Ed. 49, 3615.

Santangelo, P.G., Roland, C.M., 1998. J. Non-Cryst. Solids 235, 709.

Santangelo, P.G., Roland, C.M., 1998. Macromolecules 31, 3715.

Santangelo, P.G., Roland, C.M., 2001. Rubber Chem. Technol. 74, 69.

Santangelo, P.G., Roland, C.M., Puskas, J.E., 1999. Macromolecules 32, 1972.

Schawe, J., 1995. Thermochim. Acta 260, 16.

Schimpf, M.E., Caldwell, K., Giddings, J.C., 2000. Field-Flow Fractionation Handbook. Wiley, New York.

Schuck, P., 2000. Biophys. J. 78, 1606.

Schulten, H.-R., Plage, B., Lattimer, R.P., 1989. Rubber Chem. Technol. 62, 698.

Schulz, G.V., Altgelt, K., Cantow, H.J., 1957. Rubber Chem. Technol. 30, 805.

Scott, D.J., Harding, S.E., Rowe, A.J. (Eds.), 2005. Modern Analytical Ultracentrifugation: Techniques and Methods. Royal Society of Chemistry, UK.

Sen, S., Mabuni, C., Walsh, D., 2001. J. Appl. Polym. Sci. 82, 672.

Sharaf, M.A., Kloczkowski, A., Mark, J.E., 1995. Rubber Chem. Technol. 68, 601.

Sharp, M.A., Pranzas, P.K., Schreyer, A., 2009. Adv. Eng. Matl. 11, 441.

Shield, S.R., Ghebremeskel, G.N., 2003. J. Appl. Polym. Sci. 88, 1653.

Shimizu, T., Tsuji, M., Kohjiya, S., 1998. Mat. Sci. Res. Internat.4, 117.

Shultz, A.R., Stockmayer, W.H., 1969. Macromolecules 2, 178.

Shutilin, Y.F., 1985. Polym. Sci. USSR 27, 2386.

Shvydkaya, N.P., Shumanov, L.A., Semenova, L.P., Lykin, A.S., 1980. Kauch. Rezina 11, 19.

Simon, S.L., 2001. Thermochim. Acta 374, 55.

Sircar, A.K., 1992. Rubber Chem. Technol. 65, 503.

Sircar, A.K., In: Turi, E.A. (Ed.), Thermal Characterization of Polymeric Materials, 2nd ed., Academic Press, 1997.

Sirisinha, C., Saeoui, P., Guaysomboon, J., 2003. J. Appl. Polym. Sci. 90, 4038.

Small, P.A., 1975. Adv. Polym. Sci. 18, 1.

Smith, W.T., Patterson, J., 1986. Anal. Chem. 58, 102R.

Smitthipong, W., Gadiou, R., Vidal, L., Wagner, P., Nardin, M., 2008. Vibr. Spect. 46, 8.

Sotta, P., Deloche, B., Herz, J., Lapp, A., Durand, D., Rabadeux, J.-C., 1987. Macromolecules 20, 2769.

http://www.spectroscopynow.com

Stanley, C.B., Strey, H.H., 2003. Macromolecules 36, 6888.

Stebounova, L, Akhremitchev, B.B., Walker, G.C., 2003. Rev. Sci. Instr. 74, 3670.

Stegeman, G., Vanasten, A.C., Kraak, J.C., Poppe, H., Tijssen, R., 1994. Anal. Chem. 66, 1147.

Stepanek, P., Morkved, T.L., Krishnan, K., Lodge, T.P., Bates, F.S., 2002. Physica A 314, 41.

Stuart, B.H., 2002. Polymer Analysis. Wiley, NY.

Suarez, I., Coto, B., 2011. Eur. Polym. J. 47, 2331.

Suzuki, H., Leonis, C., Gordon, M., 1973. Makromol. Chem.172, 227.

Szep, A., Marosfoi, B., Bertalan, G., Anna, P., Marosi, G., 2003. Macromol. Symp. 202, 269.

Tacx, J., Ammerdorffer, J., German, A., 1988. Polymer 29, 2087.

Tanaka, Y., 1991. Rubber Chem. Technol. 64, 325.

Tanaka, T. (Ed.), 1999. Experimental Methods in Polymer Science. Academic Press, San Diego, CA.

Tanaka, Y., Sato, H., Adachi, J., 1987. Rubber Chem. Technol. 60, 25.

Tang, H., Liu, Z.Y., Piao, J.H., Chen, X.F., Lou, Y.X., Li, S.H., 1994. J. Appl. Polym. Sci. 51, 1159.

Tassin, J.-F., Baschwitz, A., Moise, J.-Y., Monnerie, L., 1990. Macromolecules 23, 1879.

Taylor, G.R., Darin, S.R., 1955. J. Appl. Phys. 20, 1075.

The New York Times, 1994. March 22, p. C3.

Thomas, A.G., Whittle, J.M., 1970. Rubber Chem. Technol. 43, 222.

Tinker, A.J., 1990. Rubber Chem. Technol. 63, 503.

Tinker, A.J., 1995. Rubber Chem. Technol. 68, 461.

Toki, S., Sics, I., Ran, S.F., Liu, L.Z., Hsiao, B.S., 2003. Polymer 44, 6003.

Toki, S., Takagi, R., Ito, M., Hsiao, B.S., 2011. Polymer 52, 2453.

Tomlin, D.W., Roland, C.M., 1993. Polymer 34, 2665.

Tosi, C., 1968. Adv. Polym. Sci. 5, 451.

Trabelsi, S., Albouy, P.A., Rault, J., 2003a. Macromolecules 36, 9093.

Trabelsi, S., Albouy, P.A., Rault, J., 2003b. Macromolecules 36, 7624.

Treloar, L.R.G., 1947. Trans. Faraday Soc. 43, 284.

Tulisalo, J., Seppala, J., Hastbacka, K., 1985. Macromolecules 18, 1144.

Tuminello, W., Buck, W., Kerbow, D., 1993. Macromolecules 26, 499.

Tyler, W., 1967. Rubber Chem. Technol. 40, 238.

Valic, S., Judeinstein, P., Deloche, B., 2003. Polymer 44, 5263.

Vana, P., Albertin, L., Barner, L., Davis, T.P., Barner-Kowollik, C., 2002. J. Polym. Sci. Polym. Polym. Chem. 40, 4032.

vanAsten, A.C., Kok, W.T., Tijssen, R., Poppe, H., 1996. J. Polym. Sci. Polym. Phys. 34, 297.

van Gennip, W.J.H., Thune, P.C., Dijkstra, J.B., Niemantsverdriet, J.W., 2004. Appl. Phys. Lett. 84, 1789.

Van Krevelen, D., 1990. Properties of Polymers, 3rd ed. Elsevier, Amsterdam.

Van Ooij, W.J., Rangarajan, V., 1988. Rubber Chem. Technol. 61, 594.

Vavra, J., Lapcik, J., Sabados, J., 1967. J. Polym. Sci. A-2 5, 1305.

Ver Strate, G., Cozewith, C., Ju, S., 1988. Macromolecules 21, 3360.

Vitalini, D., Scamporrino, E., 1992. Polymer 33, 4597.

Wachowicz, M., Gill, L., Wolak, J., White, J.L., 2008. Macromolecules 41, 2832.

Waddell, W.H., Parker, J.R., 1992. Rubber Chem. Technol. 65, 836.

Walton, J.H., Miller, J.B., Roland, C.M., 1992. J. Polym. Sci. Polym. Phys. 30, 527.

Walton, J.H., Miller, J.B., Roland, C.M., Nagode, J.B., 1993. Macromolecules 26, 4052.

Wang, H.T., Bethea, T., Harwood, H., 1993. Macromolecules 26, 715.

Wang, B.L., Mukataka, S., Kokufuta, E., Ogiso, M., Kodama, M., 2000. J. Polym. Sci. Polym. Phys. 38, 214.

Wang, J., Chen, B., Yan, F., Xue, Q., Zhao, F., 2011. Wear 272, 176.

Wasserman, S.H., 1995. J. Rheology 39, 601.

Weibel, E.R., 1973. In: Hoyat, M.A. (Ed.), Principles and Techniques of Electron Microscopy, vol. 3. Van Nostrand, New York (Chapter 6).

Westermann, S., Pyckhout-Hintzen, W., Richter, D., Straube, E., Egelhaaf, S., May, R., 2001. Macromolecules 34, 2186.

Westermann, S., Kreitschmann, M., Pyckhout-Hintzen, W., Richter, D., Straube, E., Farago, B., Goerigk, G., 1999. Macromolecules 32, 5793.

Wetzel, D.L., LeVine, S.M., 1999. Science 285, 1224.

Wignall, G.D., 1996. In: Mark, J.E. (Ed.), Physical Properties of Polymers Handbook, Amer. Inst. Phys. Woodbury, NY (Chapter 22).

Wild, L., 1991. Adv. Polym. Sci. 98, 1.

Williams, S.K.R., Lee, D., 2006. J. Separation Sci. 29, 1720.

Winesett, D.A., Tsou, A.H., 2008. Rubber Chem. Technol. 81, 265.

Winesett, D.A., Ade, H., Smith, A.P., Urquhart, S.G., Dias, A.J., Stevens, P., 2003. Rubber Chem. Technol. 76, 803.

Wolak, J., Jia, X., Gracz, H., Stejskal, E.O., White, J.L., Wachowicz, M., Jurga, S., 2003. Macromolecules 36, 4844.

Wu, G.L., Zeng, S.J., Ou, E.C., Yu, P.R., Xiong, Y.Q., Xu, W.J., 2011. J. Appl. Polym. Sci. 120, 1162.

Wunderlich, B., 2007. J. Appl. Polym. Sci. 105, 49.

Xu, S.H., Wells, P.S., Tao, Y.M., Yun, K.S., Parcher, J.F., 2000. ACS Symp. Series 748, 96.

Yamada, T., Okumoto, T., Ohtani, H., Tsuge, S., 1990. Rubber Chem. Technol. 63, 191.

Yamada, T., Okumoto, T., Ohtani, H., Tsuge, S., 1991. Rubber Chem. Technol. 64, 708.

Yamada, H., Manas-Zloczower, I., Feke, D.L., 1997. Powder Technol. 92, 163.

Yamakawa, H., 1971. Modern Theory of Polymer Solutions. Harper, NY.

Zaper, A.M., Koenig, J.L., 1988. Macromol. Chem. 189, 1239.

Zemel, I.S., Roland, C.M., 1992a. Polymer 33, 4522.

Zemel, I.S., Roland, C.M., 1992b. Polymer 33, 3427.

Zeng, W., Du, Y., Xue, Y., Frisch, H.L., 2006. In: Mark, J.E. (Ed.), Physical Properties of Polymers Handbook, Amer. Inst. Phys. Woodbury, NY (Chapter 17).

Zerda, T.W., Song, G., Waddell, W.H., 2003. Rubber Chem. Technol. 76, 769.

Zhang, Y.M., Ge, S., Tang, B., Koga, T., Rafailovich, M.H., Sokolov, J.C., Peiffer, D.G., Li, Z., Dias, A.J., McElrath, K.O., Lin, M.Y., Satija, S.K., Urquhart, S.G., Ade, H., Nguyen, D., 2001. Macromolecules 34, 7056.

Zhang, P., 2010. F. Zhao. Y. Yuan, X. Shi, and S. Zhao. Polymer 51, 257.

Zhang, C.H., Niu, H., Dong, J.Y., 2012. Polym. Bull. 68, 949.

Zhao, Q., Tannenbaum, R., Jacob, K.I., 2006. Carbon 44, 1740.

Zheng, Y., Turner, W., Zong, M.M., Irvine, D.J., Howdle, S.M., Thurecht, K.J., 2011. Macromolecules 44, 1347.

Zheng, Y., Thurecht, K.J., Wang, W.X., 2012. J. Polym. Sci. Polym. Chem. Ed. 50, 629.

Zheng, J., Liu, F., Lin, Y.C., Zhang, Z.J., Zhang, G.C., Wang, L., Liu, Y., Tang, T., 2012. Macromolecules 45, 1190.

Ziabicki, A., Jarecki, L., 1978. Coll. Polym. Sci. 256, 332.

Zimina, T., Fell, A., Castledine, J., 1992. Polymer 33, 4129.